QUARTERLY JOURNAL
OF THE
ROYAL METEOROLOGICAL SOCIETY

Vol. 82 APRIL 1956 No. 352

551.513.1 : 551.509.33 : 681.14

The general circulation of the atmosphere : a numerical experiment

By NORMAN A. PHILLIPS
The Institute for Advanced Study, Princeton, U.S.A.

(Manuscript received 17 October 1955)

SUMMARY

A long-period numerical forecast is made with a two-level quasi-geostrophic model, starting with an atmosphere in relative rest. Both friction and non-adiabatic effects are included in the equations, the latter as a linear function of latitude. Principal empirical elements in the experiment are the intensity of the heating, the value of the vertical stability, and the type of frictional dissipation. The flow patterns which develop are quite realistic, including a jet and zonal surface westerlies in middle latitudes, and the growth of a large disturbance. The associated energy transformations are investigated, and demonstrate the important role of the disturbance in the development of the zonal currents. The meridional circulation is also studied, together with its contribution to the zonal momentum budgets of the lower and upper halves of the atmosphere. Truncation errors eventually put an end to the forecast by producing a large fictitious increase in energy.

1. INTRODUCTION

If directly reflected radiation is omitted from consideration, the atmospheric column above each square metre of the earth's surface receives on the average about 200 joules every second in the form of solar radiation. Estimates indicate that of this absorbed energy, only about five joules are transformed into kinetic energy before being re-radiated back to space (Brunt 1944). The ultimate explanation of this inefficiency is not a simple matter, depending as it does not only on the radiative and thermodynamic properties of the atmosphere, but also on the mechanism of frictional dissipation and the dynamics of the generation of kinetic energy on various scales.

Recent years have shown some progress in our understanding of all these aspects of the problem, but perhaps the greatest relative advance has occurred in the study of the hydrodynamics of the large-scale flow patterns which are presumably responsible for the generation of kinetic energy. Increased knowledge in this field is due primarily to the extension of the aerological network between 1935 and 1945. This has led not only to greater familiarity with the actual three-dimensional atmospheric motions, but has stimulated a great deal of theoretical work looking toward their explanation. In this way, for example, some success has been obtained in the forecasting of day-to-day changes by the numerical integration of simplified forms of the hydrodynamic equations.

The properties of a rotating fluid subjected to heating and cooling have also been studied experimentally, and the results to date have contributed significantly to our information. These laboratory experiments have been carried out with water in a rotating pan, the system being heated at the outer rim and cooled at the centre (Fultz 1951, Hide 1953). In spite of the obvious dissimilarities between the laboratory set-up and the atmosphere (one has but to consider, for example, the spherical shape of the earth and the presence of water vapour in the atmosphere with its profound effect on the distribution of heating and cooling), certain of the experimental flow patterns are remarkably like those encountered on weather maps. Thus one is almost forced to the conclusion that at least the gross features of the general circulation of the atmosphere can be predicted without having to specify the heating and cooling in great detail.

This paper presents the result of an attempt to do this by means of a numerical experiment based on recent experience in numerical forecasting.

Although the emphasis will be on the interpretation of the computations as shedding some light on the general circulation, the experiment is not without significance for the more practical problem of extending the range of numerical forecasts, since a highly desirable (if not absolutely necessary) requirement of a scheme for long-range forecasting is that it be able to predict the mean state of the atmosphere. From this aspect, the computation appeared to be a logical extension of recent work on short-range numerical weather prediction, not only providing some information on the validity of the physical assumptions, but also furnishing valuable experience in the numerical problems to be encountered in making long-range predictions.

The experiment contains empirical elements in that the representation of certain physical effects is based on meteorological experience with the actual atmosphere, rather than being predicted from the fundamental laws of physics. Thus, the vertical stability is assumed equal to that of the real atmosphere, the intensity of the heating and cooling is determined from measurements of the mean non-adiabatic processes in the atmosphere, and the values of the friction coefficients are also empirical. A more complete theory of the atmospheric motions will eventually explain these quantities also.

2. A summary of present knowledge of the general circulation

Let us begin by listing some of the most striking features of the atmosphere, calling for explanation, as known from observation. (In this initial attempt at a quantitative prediction of the general circulation it is obviously wise to omit from consideration phenomena which depend on longitudinal asymmetries in the surface of the earth or represent seasonal fluctuations, realizing, however, that these also belong to the problem of the general circulation).

1. The general increase of entropy (potential temperature) with height and the existence of the stratosphere.
2. The magnitude of the poleward decrease of temperature in the troposphere, this decrease being most rapid in middle latitudes. At the 500-mb level the equator-to-pole temperature difference is approximately 45°K in winter and 22°K in summer (Hess 1948).
3. The distribution of mean zonal wind. At the surface there are easterly trade winds in subtropical latitudes, westerlies in temperate latitudes, and weaker easterlies in polar regions. The westerly component increases with height to the tropopause level, in close agreement with the geostrophic requirement of the poleward temperature decrease. In the equatorward part of those latitudes with westerly surface winds (between 35° and 40°) this increase shows up in the presence of a 'jet' at the level of the tropopause. The zonal wind speed in the climatological jet seems to be about 50 m sec^{-1} in winter and 20 m sec^{-1} in summer (Mintz 1954), although individual jets may on occasion attain speeds twice as great (Palmén 1951).
4. The travelling cyclones and anticyclones which are a prominent feature of the flow pattern in extratropical latitudes. These are usually associated with 'fronts,' characterized by a cyclonic wind shift and sudden temperature change.
5. With the exception of an equatorward drift in the surface layers of the trade-wind regions, any organized meridional circulation seems to be too small (less than 1 m sec^{-1}) to appear clearly in the available wind statistics (Starr and White 1955).

The several estimates that have been made of the distribution of radiative heating and cooling in the atmosphere all agree that if the atmosphere were in radiative equilibrium, the temperature would decrease more rapidly with height in the troposphere, and the

temperature difference between equator and pole would be larger than it is. It follows then that the atmospheric movements must on the average be such as to transport energy upward and poleward. In these elementary computations we shall not be able to predict a value of the vertical temperature gradient, the model being so crude as not even to recognize the existence of the stratosphere. However, the equations will permit a latitudinal transport of energy.

The frictional drag of the surface of the earth clearly gives rise to a positive torque (eastward acceleration) on the atmosphere in those latitudes with easterly surface winds, and a negative torque (westward acceleration) on the atmosphere in middle latitudes where westerly surface winds prevail. As was first pointed out by Jeffreys, there must therefore exist a net transfer of positive angular momentum into middle latitudes from polar and subtropical latitudes (Jeffreys 1926).

Early attempts to explain the observed distribution of surface zonal winds were based on extensions of Hadley's famous explanation of the trade winds (Hadley 1735). The motion was assumed to be independent of longitude, so that the generation of kinetic energy had to be accomplished by a direct meridional circulation. Bjerknes and collaborators have estimated the intensity of the (direct) meridional circulation of this type which would provide the required upward and poleward transport of heat on a yearly basis. The maximum meridional velocity in their calculation is about $2\frac{1}{2}$ m sec^{-1} (Bjerknes *et al.* 1933). It has long been realized that great difficulties are encountered in reconciling this simple picture with the existence of surface westerlies in middle latitudes, and that a more realistic picture can be obtained only by recognizing the contribution of the large-scale eddies to the meridional transports of energy and zonal momentum (Exner 1925).

However, the lack of aerological observations at that time precluded any quantitative examination of this process. Furthermore, a theoretical deduction of the properties of the large eddies was greatly hampered by the preoccupation of theoretical meteorologists with the difficult dynamics of the idealized polar-front discontinuity. The great increase in upper-air observations during and after the second world war not only made possible an observational verification of the important role the large disturbances play in the meridional transports of both energy and zonal momentum, but also provided the theoretician with more tractable (and realistic) equations by reducing the emphasis on the idealized polar front as a primary ingredient of extra-tropical models.

The meridional transport of zonal momentum by the eddies has been computed from observations (Widger 1949, Mintz 1955), with the result that Jeffreys' hypothesis has indeed been verified; the eddies account rather well for the total flux of zonal momentum into middle latitudes necessary to replace that lost by friction with the earth. Calculations of the poleward transport of sensible and latent heat by the eddies have also been made from observations (Starr and White 1955, Mintz 1955). In extra-tropical latitudes these transports are of the right order of magnitude to balance net radiational energy losses at high latitudes and gains at lower latitudes. (Unfortunately, the radiational gains and losses are not known well enough for a more exact comparison.)

It follows that the energetics of the large eddies must be considered together with that of the mean motion itself; the observed eddy-flux of zonal momentum into middle latitudes (where the zonal wind is a maximum) corresponding formally to a transformation of eddy kinetic energy into the kinetic energy of zonal motion (Starr 1953). However, the necessary generation of kinetic energy from potential energy (we use the term potential energy to include both gravitational energy and internal energy, since the latter is related uniquely to the former in a hydrostatic atmosphere) is difficult to study observationally, since it essentially requires a knowledge of the field of vertical motion, although some

attempts have been made (Phillips 1949, Spar 1950, Palmén and Newton 1951). Here theory has been of great value, and the several theories of the instability of waves in a baroclinic zonal current (Charney 1947, Eady 1949, Fjørtoft 1950, Kuo 1952) have predicted that the large-scale disturbances of extratropical latitudes not only transport heat poleward and upward, but also generate kinetic energy, this energy coming primarily from the potential energy represented by the latitudinal temperature gradient.

In tropical latitudes on the other hand, the existence of the Hadley type of circulation seems to be borne out not only by direct observations (Riehl and Yeh 1950, Palmén 1955, Starr and White 1955), but also indirectly through the failure in low latitudes of the large-scale eddy mechanism to provide a sufficiently large poleward transport of energy (Starr and White 1955). The importance of the simple meridional type of circulation in low latitudes is also suggested by theory (Kuo 1954) and experiment (Hide 1953).

3. The equations

The vague outlines of a consistent theory of the general circulation have thus been gradually appearing during the last decade; in extra-tropical latitudes the large-scale turbulence is dominant (Eady 1950), while in low latitudes a more classical scheme seems to be indicated.

The large-scale motions in extra-tropical latitudes are quasi-geostrophic in character, and the geostrophic theory has been used with some success to forecast the flow-pattern changes from day to day. Although the equations used to date for this purpose have in general not included the effects of non-adiabatic heat changes and friction, it is possible to incorporate them in a crude manner. One can then test the extent to which the geostrophic theory is capable of explaining the observed general circulation as the result of a prescribed distribution of heat and cold sources, simply by making a ' forecast ' for a long period, starting, for example, with a resting atmosphere. Certain reservations are necessary in low latitudes, where the geostrophic theory is inadequate, but the results of all the perturbation studies of the last decade indicate that some success should attend a numerical experiment of this type (see especially Charney 1951).

The 2-level geostrophic model is perhaps the simplest model which would seem capable of incorporating the effects of both heating and friction. In deriving the equations for a simplified version of this model, we find it convenient to use the x, y, p, t-coordinate system (Eliassen 1949), and neglect the purely kinematic effects of the curvature of the earth. The following notation will be used :

x = distance coordinate to east
y = distance coordinate to north
p = pressure (the vertical coordinate)
t = time
(u, v, ω) = time rates of change of (x, y, p) following the motion
Φ = latitude
ϕ = geopotential ($= gz$ where z is height)
$\mathbf{V}$ = horizontal velocity vector
f = Coriolis parameter $= 2\Omega \sin \Phi$
A_v = lateral kinematic eddy-viscosity coefficient
A_T = lateral eddy-diffusion coefficient for heat
τ_x, τ_y = x and y components of the frictional (small-scale) stress acting across a horizontal surface
θ = potential temperature
dQ/dt = non-adiabatic rate of heating per unit mass

T = temperature
∇ = horizontal gradient operator on an isobaric surface
c_p, c_v = specific heats of air at constant pressure and volume
$R = c_p - c_v$
$\beta = df/dy$, Rossby's parameter $= 2\Omega a^{-1} \cos \Phi$
a = radius of the earth
Ω = rotation of the earth
g = acceleration of gravity
p_4 = pressure at the ground (assumed constant and equal to 1,000 mb)
ρ = density

The (approximate) equations of motion and continuity in this system are

$$\partial u/\partial t + \mathbf{V} \cdot \nabla u - fv = - \partial\phi/\partial x + A_v \nabla^2 u + g \, \partial\tau_x/\partial p \, . \quad (1)$$

$$\partial v/\partial t + \mathbf{V} \cdot \nabla v + fu = - \partial\phi/\partial y + A_v \nabla^2 v + g \, \partial\tau_y/\partial p, \quad (2)$$

$$\nabla \cdot \mathbf{V} + \partial\omega/\partial p = 0, \quad (3)$$

and the thermodynamic energy equation is

$$\frac{1}{c_p T} \frac{dQ}{dt} = \frac{d \ln \theta}{dt} = \left(\frac{\partial}{\partial t} + \mathbf{V} \cdot \nabla + \omega \frac{\partial}{\partial p} \right) \ln \theta \quad (4)$$

In eqs. (1) and (2) we have neglected principally the terms $\omega \, \partial u/\partial p$ and $\omega \, \partial v/\partial p$.

The 2-level model we will use represents the flow pattern in the upper half of the atmosphere by that at the 250-mb level, and the flow pattern in the lower half of the atmosphere by that at the 750-mb level (Charney and Phillips 1953). For convenience we designate quantities measured at the 0-, 250-, 500-, 750-, and 1,000-mb levels by the subscripts 0, 1, 2, 3, and 4, respectively. As boundary conditions at the top and bottom we will take

$$\omega = 0 \text{ at } p = 0 \text{ and } p = p_4. \quad (5)$$

τ_x and τ_y necessarily vanish at $p = 0$, but unfortunately practically nothing is known about their value at 500 mb. We will therefore assume that they are much smaller at 500 mb than at 1,000 mb and set them equal to zero at level 2. At the ground level the stress is generally taken to be directed opposite to the surface wind C, and proportional to the square of the wind speed at anemometer height, according to the formula

$$|\tau_4| = \kappa \rho C^2$$

with a value of about 0·003 for the non-dimensional constant κ. For simplicity, however, we will assume that τ_4 is directed at a constant angle to the surface geostrophic wind, and is proportional to the first power of the speed. Assuming further that the anemometer wind speed is about 70 per cent of the geostrophic wind speed we can write

$$\frac{g}{p_2} \left(\frac{\partial\tau_y}{\partial x} - \frac{\partial\tau_x}{\partial y} \right)_4 = - k \zeta_4, \quad (6)$$

where the constant k is given by

$$k = 0{\cdot}98 \, g \, \kappa \, \overline{C}_g \, (RT_4)^{-1}. \quad (7)$$

$\overline{C}_g$ is a characteristic value of the surface geostrophic wind speed, and ζ_4 is the surface geostrophic vorticity. k takes the value 4×10^{-6} sec^{-1} if we take $\overline{C}_g$ to be about 11 m sec^{-1}.

The quasi-geostrophic vorticity equations for our model will be obtained by cross differentiation of Eqs. (1) and (2) at levels 1 and 3, with the geostrophic assumption introduced in the result for all velocities except those in the term $f \nabla \cdot \mathbf{V}$. For this term we

will substitute from the equation of continuity (3), with $\partial\omega/\partial p$ at levels 1 and 3 evaluated by taking centred finite differences, $(\partial\omega/\partial p)_1 \simeq (\omega_2 - \omega_0)/p_2$ and $(\partial\omega/\partial p)_3 \simeq (\omega_4 - \omega_2)/p_2$. Since ω_0 and ω_4 vanish, this gives us

$$\nabla \cdot \mathbf{V}_1 = -\nabla \cdot \mathbf{V}_3 = -\omega_2/p_2. \quad . \quad . \quad . \quad (8)$$

The p derivatives of the stress τ will also be evaluated by finite differences. Since the stress vanishes at levels 0 and 2, we find that it does not appear in the vorticity equation at level 1, and only the curl of the surface stress, Eq. (6), appears in the vorticity equation for level 3.

$$(\partial/\partial t + \mathbf{V}_1 \cdot \nabla)(f + \zeta_1) - f\,\omega_2/p_2 = A_v \nabla^2 \zeta_1 \quad . \quad . \quad . \quad (9)$$

$$(\partial/\partial t + \mathbf{V}_3 \cdot \nabla)(f + \zeta_3) + f\,\omega_2/p_2 = A_v \nabla^2 \zeta_3 - k\,\zeta_4. \quad . \quad . \quad (10)$$

The thermodynamic energy equation will be written at level 2. Introducing finite differences of the form $(\phi_3 - \phi_1)/p_2 \sim (\partial\phi/\partial p)_2$ and using the relation

$$\theta = \partial\phi/\partial p \times \text{a function of pressure},$$

and the hydrostatic equation

$$\partial\phi/\partial p = -RT/p \quad . \quad . \quad . \quad . \quad . \quad (11)$$

we may write Eq. (4) in the form

$$\frac{\omega_2}{p_2}\left[\frac{\theta_1 - \theta_3}{\theta_2}\right](\phi_1 - \phi_3) = \left(\frac{\partial}{\partial t} + \mathbf{V} \cdot \nabla\right)(\phi_1 - \phi_3) - \frac{R}{c_p}\left(\frac{dQ}{dt}\right). \quad . \quad (12)$$

The 2-level model is incapable of forecasting changes in the vertical stability parameter $(\theta_1 - \theta_3)/\theta_2$ and we must therefore take this to be a constant. Furthermore, since the percentage variation in $(\phi_1 - \phi_3)$ is far less than that of ω_2, we will also take $(\phi_1 - \phi_3)$ to be a constant on the *left* side of Eq. (12). ϕ_1 and ϕ_3 when they appear elsewhere in the equations, may then be considered as deviations from the standard atmosphere values.

Strictly speaking (dQ/dt) in Eq. (12) is the non-adiabatic rate of heating per unit mass at the 500-mb level. However, the crudeness of the 2-level model strongly suggests that this should be interpreted rather as the average non-adiabatic heating throughout an entire column of the atmosphere, and we can therefore neglect the contribution from the vertical transport of heat by small-scale turbulence. The remaining important physical processes determining dQ/dt are the release of latent heat, radiation, and lateral eddy diffusion on a scale smaller than that of the large disturbances (the latter being forecast in detail).

Evaporation and condensation have the effect of reducing the effective vertical stability $(\theta_1 - \theta_3)/\theta_2$ in regions of saturation. Furthermore, a net excess of condensation over evaporation in a given latitude belt corresponds to a non-adiabatic heating of the atmosphere in that latitude belt. Since we do not wish to encumber our model at this time with the details of the water budget, we will allow for the release of latent heat only qualitatively by reducing the stability factor $(\theta_1 - \theta_3)/\theta_2$ in Eq. (12) to 80 per cent of its value in the standard atmosphere, and at the same time reducing the latitudinal gradient of heating to allow roughly for the observed latitudinal transport of latent heat.

Fig. 1 summarizes several calculations of the latitudinal energy transports needed to balance the estimated annual gains and losses of energy by radiation. Although they all agree that the maximum transport should occur between 30° and 40°, the largest values (Houghton's and Simpson's) and the smallest values (Albrecht's and London's) differ by a factor of two. Fig. 2 summarizes various calculations of the *observed* latitudinal transports of energy in the form of sensible and latent heat. (The transport of potential energy is impossible to compute on a geostrophic basis since it can only be accomplished

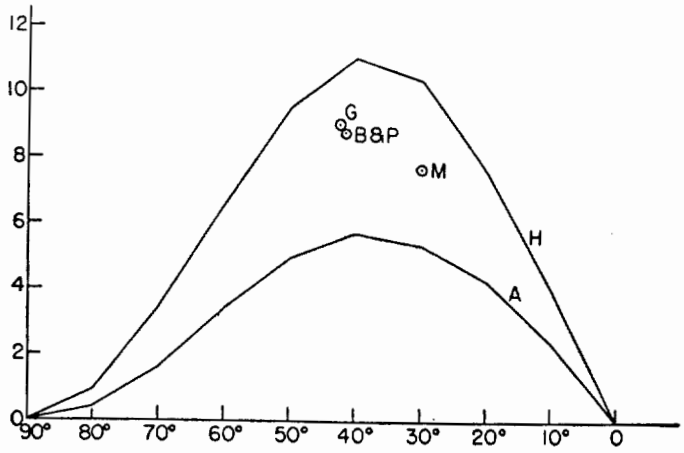

Figure 1. Poleward transport of energy across entire latitude circles required to balance radiational excesses and deficits in the annual mean. Units are 10^{19} cal day^{-1}. Curves H and A are the values obtained by Houghton (1954) and Albrecht (1931). The position of the maxima of the curves deduced by Gabites (1950), Baur and Philipps (1935), and Möller (1950) are indicated by the circles. The results of Simpson (1929) and London (1951) agree almost identically with those of Houghton and Albrecht, respectively.

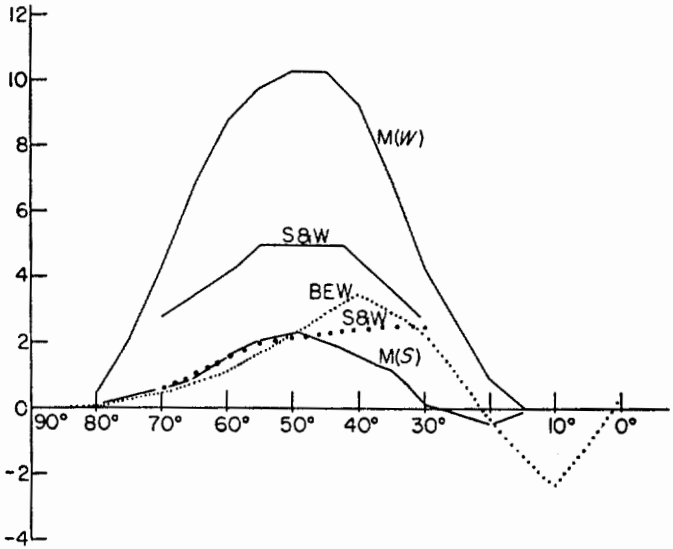

Figure 2. Observed poleward transports by eddies of sensible heat (full curves) and latent heat (dotted curves). Units are 10^{19} cal day^{-1}. M (W) and M (S) are Mintz's geostrophic measurements for winter and summer (Mintz 1955), the full curve S & W that of Starr and White (1955) for the annual mean. The dotted curve S & W is the measurement by Starr and White (*ibid.*) of the annual eddy transport of latent heat. The dotted curve BEW is the average of the estimate by Benson and Estoque and that of Wüst for the total transport of latent heat (Benson and Estoque 1954).

by a mean meridional circulation (Starr 1951), and the latitudinal transport of kinetic energy is negligible). A comparison of Figs. 1 and 2 shows that a considerable portion of the necessary transport is accomplished by eddies in middle and high latitudes, even if the larger 'radiative' values are accepted, while in lower latitudes some other mechanism seems to be necessary. (This may very well be accomplished by a direct meridional circulation at low latitudes. Palmén and Alaka (1952) have shown how such a cell fits in very well with the angular momentum budget at those latitudes, and Palmén has also demonstrated that it is quite consistent with the water budget of the doldrum belt).

Before determining the intensity of heating to use in our calculations, it is necessary to fix the geometry of the region containing our experimental 2-level atmosphere. We take the simplest conceivable arrangement, namely a rectangular region, limited by 'walls' at $y = \pm W$, but open at the western and eastern sides ($x = 0$ and L), where we impose the condition that the flow at $x = 0$ is identical with that at $x = L$ (cyclic continuity). The 'radiative' energy gains and losses will be specified as a *linear function of y*,

$$\left(\frac{dQ}{dt}\right)_{\text{rad}} = -2H(y/W). \quad . \quad . \quad . \quad . \quad (13)$$

The constant H is the mean rate of heating per unit mass from $y = -W$ to $y = 0$ (or cooling from $y = 0$ to $y = W$). This heating will thus be independent of the motion. This condition is fulfilled neither in the dishpan experiments nor in the actual atmosphere but seems to be a reasonable first approximation.

The geometry of the sphere being different from that of our region, the determination of an appropriate value of H from curves of the type given in Figs. 1 and 2 is somewhat arbitrary. In the model the rate of energy transport across the line $y = 0$ from $x = 0$ to $x = L$ must be equal to $HWL\,p_4/g$ kj sec^{-1} if a steady state is to be attained. For every metre of this line, then, the rate of energy transport in a steady state must be $HW\,p_4/g$ kj m^{-1} sec^{-1}. The observed rate of eddy transport of sensible heat in the atmosphere at 45° latitude is about 6×10^{19} cal day^{-1}, or about 10^5 kj sec^{-1} per metre of length of the 45° latitude circle. Taking $W = 5 \times 10^6$ m (approximately half the pole-to-equator distance on the earth) we find by equating these values,

$$H \simeq 2 \times 10^{-3} \text{ kj ton}^{-1} \text{ sec}^{-1}. \quad . \quad . \quad . \quad (14)$$

Since the total eddy transport of sensible and latent heat according to Fig. 2 is about equal to the mean of the radiation figures at 45°, this value of H also corresponds roughly to the observed radiation effects minus the observed convergence of latent heat transport.

The effect of lateral eddy diffusion on dQ/dt will be represented by

$$\left(\frac{dQ}{dt}\right)_{\text{diff}} = c_p A_T \nabla^2 T_2 = \frac{c_p}{R} A_T \nabla^2 (\phi_1 - \phi_3). \quad . \quad . \quad (15)$$

We now make the assumption that f is a constant (equal to f_0) everywhere, except when it is differentiated with respect to y in Eqs. (9) and (10), where, following Rossby (1939) we assume that $df/dy \equiv \beta = \text{constant}$.

Eqs. (9), (10) and (12) take a simpler form if we define a 'stream function' for the geostrophic wind,

$$\psi_1 = \phi_1/f_0, \qquad \psi_3 = \phi_3/f_0$$

and introduce the parameter

$$\lambda^2 = f_0^2\,\theta_2\left[(\phi_1 - \phi_3)(\theta_1 - \theta_3)\right]^{-1} = \text{constant}. \quad . \quad . \quad (16)$$

Eqs. (9), (10), and (12) may then be rewritten

$$(\partial/\partial t + \mathbf{V}_1 \cdot \nabla)(\beta y + \zeta_1) - f_0\,\omega_2/p_2 = A_v \nabla^2 \zeta_1, \quad . \quad . \quad . \quad (17)$$

$$(\partial/\partial t + \mathbf{V}_3 \cdot \nabla)(\beta y + \zeta_3) + f_0\,\omega_2/p_2 = A_v \nabla^2 \zeta_3 - k\,\zeta_4, \quad . \quad . \quad (18)$$

$$\frac{f_0\,\omega_2}{p_2} = \lambda^2\left[\left(\frac{\partial}{\partial t} + \mathbf{V} \cdot \nabla\right)(\psi_1 - \psi_3) + \frac{2RH}{f_0\,c_p} \cdot \frac{y}{W} - A_T \nabla^2 (\psi_1 - \psi_3)\right]. \quad . \quad (19)$$

Relatively little is known about the appropriate values for A_v and A_T. In our case they represent the effect of eddies smaller than the grid size used in the computations. Application of Richardson's empirical law $A \sim 0{\cdot}2\, l^{4/3}$ (Richardson 1926, Batchelor 1950), with l equal to $\Delta x \sim 3{\cdot}10^7$ cm (300 km) gives a value of about 10^5 m^2 sec^{-1} for A. In terms of the usual mixing length hypothesis, $A \sim \overline{vl}$, this corresponds to an effective (small-scale) eddy velocity of less than 1 m sec^{-1}. Machta has recently reported on a study of the lateral spread of radioactive dust from atomic explosions (Machta 1955), and deduced a value of A of about $\frac{1}{2}$ of this value (assuming Fickian diffusion of the dust cloud). Grimminger's computations of the lateral spread of mixing ratio lines on isentropic charts (Grimminger 1938) correspond to values of A from 10^4 to 10^6 m^2 sec^{-1}. Lacking any empirical or theoretical basis for a more definite choice for A_v and A_T, we shall set them both equal to

$$A_v = A_T = A = 10^5 \text{ m}^2 \text{ sec}^{-1}. \qquad (20)$$

We note in passing that this is about 1/40th of the value of A necessary to explain the heat transport required in Fig. 1 as a large-scale *austausch* process (Defant 1921), and it will therefore not balance the radiative heating by itself unless the latitudinal temperature gradient is 40 times as large as normal.

Eqs. (17), (18) and (19) are now in a form suitable for application of normal numerical forecasting techniques, if we assume that the vorticity at level 4, ζ_4, is defined by linear extrapolation from levels 1 and 3,

$$\zeta_4 = \tfrac{3}{2}\,\zeta_3 - \tfrac{1}{2}\,\zeta_1 \,. \qquad (21)$$

and measure $\mathbf{V}$ and ζ by the geostrophic relation $u = -\,\partial\psi/\partial y$, $v = \partial\psi/\partial x$.

An efficient forecast scheme is obtained by defining the ' relative potential vorticities ' at levels (1) and (3)

$$q_1 = \zeta_1 - \lambda^2(\psi_1 - \psi_3) = \nabla^2\psi_1 - \lambda^2(\psi_1 - \psi_3), \qquad (22)$$

$$q_3 = \zeta_3 + \lambda^2(\psi_1 - \psi_3) = \nabla^2\psi_3 + \lambda^2(\psi_1 - \psi_3), \qquad (23)$$

whereupon Eqs. (17)-(19) can be thrown into the forms :

$$\frac{\partial q_1}{\partial t} = -\,\mathbf{V}_1 \cdot \nabla(\beta y + q_1) + A\nabla^2 q_1 + \left(\frac{2RH\lambda^2}{f_0 c_p}\right)\left(\frac{y}{W}\right) \qquad (24)$$

$$\frac{\partial q_3}{\partial t} = -\,\mathbf{V}_3 \cdot \nabla(\beta y + q_3) + A\nabla^2 q_3 - \left(\frac{2RH\lambda^2}{f_0 c_p}\right)\left(\frac{y}{W}\right) - \frac{k}{2}[3q_3 - q_1 - 4\lambda^2(\psi_1 - \psi_3)]. \qquad (25)$$

Thus, if q and ψ are known at time t, Eqs. (24) and (25) give the values of $\partial q/\partial t$, so that values of q at $t + \Delta t$ may be obtained by extrapolation. Eqs. (22) and (23) then allow ψ_1 and ψ_3 to be determined at $t + \Delta t$ from the values of $q\,(t + \Delta t)$. Some caution must be used, however, in this scheme, and the actual numerical method is described in detail in the appendix.

The method of solution requires that certain boundary conditions are given at the boundaries of the rectangular region $0 \leqslant x \leqslant L$, $-\,W \leqslant y \leqslant W$. At $x = 0$ and $x = L$, as stated before, we merely require cyclic continuity – that is, we imagine that there is an infinite number of such rectangular regions along the x-axis, each undergoing the same motions.

At $y = \pm\, W$, the boundary conditions are not so obvious. In the usual method of making numerical forecasts, arbitrary conditions are specified on the lateral boundaries,

and the portion of the region in which the forecast is valid shrinks with time because of these incorrect boundary conditions. In our case, where we intend to make a forecast for an extended period, it is obvious that this luxury cannot be enjoyed, and the boundary conditions at the walls ($y = \pm W$) must in some sense be stated correctly. Now the 'walls' are primarily a mathematical device to limit the motion, having no counterpart on the earth, and the geostrophic assumption seems to confuse the straightforward application of the physical conditions applying at real walls (Charney 1955), so that the boundary conditions we shall use there are somewhat heuristic in character. However, as will be seen in the next section, they lead to meaningful statements with regard to the energy and momentum integrals of the flow.

We first introduce the concept of the *mean* and *disturbed* flow, by defining

$$\bar{\psi}(y, t) \equiv \frac{1}{L}\int_0^L \psi(x, y, t)\, dx \quad . \quad . \quad . \quad . \quad (26)$$

as the *mean* value of ψ, and

$$\psi'(x, y, t) \equiv \psi(x, y, t) - \bar{\psi}(y, t) \quad . \quad . \quad . \quad (27)$$

as the *disturbance* value of ψ. This definition is, of course, readily extendable to other quantities such as q, ζ, u, v, ω, etc., as well as to their products.

An obvious first requirement is that

$$\psi' \equiv 0 \quad \text{at} \quad y = \pm W, \quad . \quad . \quad . \quad . \quad (28)$$

this corresponding to the statement that the normal geostrophic velocity vanishes at the wall. Another requirement we will impose somewhat arbitrarily is that

$$\zeta' \equiv 0 \quad \text{at} \quad y = \pm W. \quad . \quad . \quad . \quad . \quad (29)$$

Integration of Eq. (1) with respect to x at the walls, using cyclic continuity and the fact that v vanishes there, leads to the relations

$$\left.\begin{aligned} \partial \bar{u}_1/\partial t &= -\partial^2 \bar{\psi}_1/\partial y\, \partial t = A\, \partial^2 \bar{u}_1/\partial y^2 \\ \partial \bar{u}_3/\partial t &= -\partial^2 \bar{\psi}_3/\partial y\, \partial t = A\, \partial^2 \bar{u}_3/\partial y^2 - \tfrac{1}{2} k (3\bar{u}_3 - \bar{u}_1). \end{aligned}\right\} \quad . \quad . \quad (30)$$

We will assume that for all t,

$$\partial^2 \bar{u}/\partial y^2 \equiv 0 \quad \text{at} \quad y = \pm W, \quad . \quad . \quad . \quad (31)$$

so that if $\bar{u}_1$ and $\bar{u}_3$ are initially zero at the walls, they must then remain zero, according to Eq. (30). The final boundary condition at the walls is therefore

$$\partial \bar{\psi}/\partial y \equiv 0 \quad \text{at} \quad y = \pm W. \quad . \quad . \quad . \quad (32)$$

Because of the linearizing assumption concerning $(\phi_1 - \phi_3)$ which was made on the left side of Eq. (12), the dependent variables ψ_1 and ψ_3 in Eqs. (17)-(32) appear only in differentiated form or in the combination $(\psi_1 - \psi_3)$. We are therefore at liberty to fix the value of (for example) $\bar{\psi}_3$ at $y = -W$. This, together with Eqs. (22)-(25) and the boundary conditions Eqs. (28)-(32), is sufficient to determine the motion completely.

It will be noticed that this set of equations and boundary conditions possesses a certain symmetry. If ψ at the initial time has the symmetry $\psi(x, y, t_0) \equiv -\psi(x - L/2, -y, t_0)$, then this symmetry will be preserved. Thus, for example, $\bar{u}(y, t) = -\partial \bar{\psi}/\partial y$ would be an *even* function of y and $(\bar{\psi}_1 - \bar{\psi}_3)(y, t)$ would be an *odd* function of y for all t. Any deviations of the actual forecast $\bar{u}$ and $(\bar{\psi}_1 - \bar{\psi}_3)$ (mean temperature) from

this symmetry therefore depend completely on the deviation of the *initial* flow pattern from the symmetrical one (or on round-off errors), and do not necessarily represent anything real. This property was not used explicitly in the computation; the approximate symmetry maintained during its course served as a crude check on the calculations.

4. Equations for the meridional circulation and energy transformations

The writer has recently shown how the simple quasi-geostrophic Eqs. (22)-(25) and the boundary conditions Eqs. (28)-(32), without friction and heating, may be used to form the energy equations for this model, and how the implied meridional circulation may be computed (Phillips 1954). We shall now derive these results for the non-adiabatic case with friction of the type included in Eqs. (24) and (25).

We first write Eqs. (17)-(19) in their averaged form,

$$\partial^2 (\partial \bar{\psi}_1/\partial t)/\partial y^2 - \bar{\omega}_2 f_0/p_2 = A\, \partial^2 \bar{\zeta}_1/\partial y^2 - \overline{\mathbf{V}_1' \cdot \nabla \zeta_1'}, \quad . \quad . \quad . \quad (33)$$

$$\partial^2 (\partial \bar{\psi}_3/\partial t)/\partial y^2 + \bar{\omega}_2 f_0/p_2 = A\, \partial^2 \bar{\zeta}_3/\partial y^2 - \overline{\mathbf{V}_3' \cdot \nabla \zeta_3'} - k\, \bar{\zeta}_4, \quad . \quad . \quad (34)$$

$$\frac{\bar{\omega}_2 f_0}{p_2} = \lambda^2 \left[\frac{\partial (\bar{\psi}_1 - \bar{\psi}_3)}{\partial t} + \overline{\mathbf{V}_1' \cdot \nabla (\psi_1' - \psi_3')} + \frac{2RH}{f_0 c_p} \cdot \frac{y}{W} - A \frac{\partial^2 (\bar{\psi}_1 - \bar{\psi}_3)}{\partial y^2} \right], \quad (35)$$

and then subtract these from Eqs. (17)-(19) to get the deviation form :

$$\nabla^2 \partial \psi_1'/\partial t - \omega_2' f_0/p_2 = A\, \nabla^2 \zeta_1' - [\mathbf{V}_1 \cdot \nabla (\beta y + \zeta_1)]', \quad . \quad . \quad (36)$$

$$\nabla^2 \partial \psi_3'/\partial t + \omega_2' f_0/p_2 = A\, \nabla^2 \zeta_3' - [\mathbf{V}_3 \cdot \nabla (\beta y + \zeta_3)]' - k\, \zeta_4', \quad . \quad (37)$$

$$\frac{\omega_2' f_0}{p_2} = \lambda^2 \left\{ \frac{\partial (\psi_1' - \psi_3')}{\partial t} + [\mathbf{V}_1 \cdot \nabla (\psi_1 - \psi_3)]' - A\, \nabla^2 (\psi_1' - \psi_3') \right\}. \quad . \quad (38)$$

We obtain four energy equations in the following way. First multiply Eq. (33) by $-\bar{\psi}_1$ and Eq. (34) by $-\bar{\psi}_3$, and integrate the sum of the two resulting equations over the entire region, invoking the boundary conditions as needed. This gives an equation for the time rate of change of the *kinetic energy of the mean zonal flow*, $\bar{K}$:

$$\left.\begin{aligned} &\partial \bar{K}/\partial t \equiv \partial/\partial t \int \tfrac{1}{2} (\bar{u}_1^2 + \bar{u}_3^2)\, d\sigma = \\ &= -(f_0/p_2) \int \bar{\omega}_2 (\bar{\psi}_1 - \bar{\psi}_3)\, d\sigma - A \int (\bar{\zeta}_1^2 + \bar{\zeta}_3^2)\, d\sigma - \\ &\quad - k \int \bar{u}_3\, \bar{u}_4\, d\sigma - \int \left[\bar{u}_1 \frac{\partial (\overline{u_1' v_1'})}{\partial y} + \bar{u}_3 \frac{\partial (\overline{u_3' v_3'})}{\partial y} \right] d\sigma. \end{aligned}\right\} \quad . \quad (39)$$

($d\sigma$ is the area element $dx\, dy$). We then follow a similar procedure with Eq. (36) and Eq. (37), multiplying them by $-\psi_1'$ and $-\psi_3'$, adding and integrating. This results in an equation for the time rate of change of the *kinetic energy of the disturbed flow*, K'. After some manipulation we find :

$$\left.\begin{aligned} &\partial K'/\partial t \equiv \partial/\partial t \int \tfrac{1}{2} [(\nabla \psi_1')^2 + (\nabla \psi_3')^2]\, d\sigma = \\ &= -(f_0/p_2) \int \omega_2' (\psi_1' - \psi_3')\, d\sigma - A \int [(\zeta_1')^2 + (\zeta_3')^2]\, d\sigma - \\ &\quad - k \int \mathbf{V}_3' \cdot \mathbf{V}_4'\, d\sigma + \int \left[\bar{u}_1 \frac{\partial (\overline{u_1' v_1'})}{\partial y} + \bar{u}_3 \frac{\partial (\overline{u_3' v_3'})}{\partial y} \right] d\sigma. \end{aligned}\right\} \quad . \quad (40)$$

Equations for the time rate of change of potential energy are obtained from Eq. (35) and Eq. (38) by multiplying these with $(\bar{\psi}_1 - \bar{\psi}_3)$ and $(\psi_1' - \psi_3')$, respectively, before integrating over the region. Eq. (35) gives the following equation for the rate of change of the *potential energy of the mean flow*, $\bar{P}$:

$$\left.\begin{aligned} &\partial\bar{P}/\partial t \equiv \tfrac{1}{2}\lambda^2\,\partial/\partial t\int(\bar{\psi}_1 - \bar{\psi}_3)^2\,d\sigma = \\ &= (f_0/p_2)\int\bar{\omega}_2\,(\bar{\psi}_1 - \bar{\psi}_3)\,d\sigma + \lambda^2\int\overline{v_1'\,(\psi_1' - \psi_3')}\,\partial\,(\bar{\psi}_1 - \bar{\psi}_3)/\partial y\,d\sigma - \\ &- (2RH\lambda^2/f_0\,c_p)\int\left(\frac{y}{W}\right)(\bar{\psi}_1 - \bar{\psi}_3)\,d\sigma - \lambda^2 A\int\left[\frac{\partial\,(\bar{\psi}_1 - \bar{\psi}_3)}{\partial y}\right]^2 d\sigma. \end{aligned}\right\} \quad (41)$$

Eq. (38) gives an equation for the time rate of change of the *potential energy of the disturbed motion*, P' :

$$\left.\begin{aligned} &\partial P'/\partial t \equiv \tfrac{1}{2}\lambda^2\,\partial/\partial t\int(\psi_1' - \psi_3')^2\,d\sigma = \\ &= (f_0/p_2)\int\omega_2'\,(\psi_1' - \psi_3')\,d\sigma - \lambda^2\int\overline{v_1'(\psi_1' - \psi_3')}\,\partial\,(\bar{\psi}_1 - \bar{\psi}_3)/\partial y\,d\sigma - \\ &\qquad - \lambda^2 A\int[\nabla\,(\psi_1' - \psi_3')]^2\,d\sigma. \end{aligned}\right\} \quad (42)$$

The combined energy equation is obtained by adding Eqs. (39)-(42) :

$$\left.\begin{aligned} &\partial\,(\bar{P} + P' + \bar{K} + K')/\partial t = -A\int(\zeta_1^2 + \zeta_3^2)\,d\sigma - \\ &- A\int[\nabla\,(\psi_1 - \psi_3)]^2\,d\sigma - k\int\mathbf{V}_3\cdot\mathbf{V}_4\,d\sigma - \frac{2RH\lambda^2}{f_0\,c_p}\int\left(\frac{y}{W}\right)(\bar{\psi}_1 - \bar{\psi}_3)\,d\sigma. \end{aligned}\right\} \quad (43)$$

According to this, the total change in energy in our model is given by

(a) A loss of energy due to the lateral eddy viscosity A. This is always a loss.

(b) A change due to the effect of surface friction, k. This is usually a loss since $\mathbf{V}_4$ and $\mathbf{V}_3$ tend to have the same direction.

(c) A change due to the non-adiabatic heating, H. This is an increase in energy when the heating is positively correlated with the temperature (the latter being proportional to $\psi_1 - \psi_3$).

It will be recalled from Eq. (13) that the total amount of heat energy added is zero. However, this can result in an increase of *available* potential energy in the model if the heat is added at high temperature and taken away at low temperatures – formally a *decrease* in the entropy of the system.

A more instructive breakdown of the energy transformations is given, however, by the four individual Eqs. (39)-(42). We notice that there are four terms which appear twice in the four equations, once with a positive sign and once with a negative sign. These terms can be considered as representing a transformation of energy from one form to another. To bring this out more clearly we first introduce symbolic notation of the form $\{\bar{P}\cdot\bar{K}\}$ to represent the various quantities on the right sides of Eqs. (39)-(42), the notation signifying a transformation of energy from one form – the first in the bracket – to the second form (Blackadar 1955).

$$
\left.
\begin{aligned}
\{\overline{Q}\cdot\overline{P}\} &\equiv -\frac{2RH\lambda^2}{f_0 c_p}\int\frac{y}{W}(\overline{\psi}_1-\overline{\psi}_3)\,d\sigma\\
\{\overline{P}\cdot P'\} &\equiv -\lambda^2\int\overline{[v_1'(\psi_1'-\psi_3')]}\,\frac{\partial(\overline{\psi}_1-\overline{\psi}_3)}{\partial y}\,d\sigma\\
\{P'\cdot K'\} &\equiv -\frac{f_0}{p_2}\int\omega_2'(\psi_1'-\psi_3')\,d\sigma\\
\{K'\cdot\overline{K}\} &\equiv -\int\left[\bar{u}_1\frac{\partial\overline{(u_1'v_1')}}{\partial y}+\bar{u}_3\frac{\partial\overline{(u_3'v_3')}}{\partial y}\right]d\sigma\\
\{\overline{P}\cdot\overline{K}\} &\equiv -\frac{f_0}{p_2}\int\overline{\omega}_2(\overline{\psi}_1-\overline{\psi}_3)\,d\sigma.\\
\{\overline{K}\cdot A\} &\equiv A\int(\overline{\zeta}_1^2+\overline{\zeta}_3^2)\,d\sigma\\
\{K'\cdot A\} &\equiv A\int[(\zeta_1')^2+(\zeta_3')^2]\,d\sigma\\
\{\overline{P}\cdot A\} &\equiv \lambda^2 A\int\left[\frac{\partial(\overline{\psi}_1-\overline{\psi}_3)}{\partial y}\right]^2 d\sigma\\
\{P'\cdot A\} &\equiv \lambda^2 A\int[\nabla(\psi_1'-\psi_3')]^2\,d\sigma\\
\{\overline{K}\cdot k\} &\equiv k\int\bar{u}_3\bar{u}_4\,d\sigma\\
\{K'\cdot k\} &\equiv k\int\mathbf{V}_3'\cdot\mathbf{V}_4'\,d\sigma
\end{aligned}
\right\}\quad . \qquad (44)
$$

The physical interpretation of these expressions is quite clear. First we note that the expression for the potential energy of the model consists essentially of the integral of the square of the temperature deviations (at 500 mb) from the standard atmosphere value. Lorentz, in a beautiful attempt to reconcile the synoptic meteorologist's intuitive association of *available* potential energy with temperature *gradients*, has recently shown how a similar expression can be approximated from the usual definition of the potential plus internal energy of the atmosphere as the volume integral of $\rho(\phi + c_v T)$ (Lorentz 1955).

$\{\overline{P}\cdot P'\}$ represents a transformation of mean potential energy into the disturbance potential energy. This is accomplished by the horizontal transport of sensible heat by the disturbance velocity v_1' [or v_3', since $\mathbf{V}_1'\cdot\nabla(\psi_1'-\psi_3')\equiv\mathbf{V}_3'\cdot\nabla(\psi_1'-\psi_3')$] from warmer to colder regions. The transformations of potential into kinetic energy, $\{\overline{P}\cdot\overline{K}\}$ and $\{P'\cdot K'\}$, represent the effect of vertical circulations in *meridional* and *zonal* planes, respectively. The transformation of disturbance kinetic energy into the kinetic energy of the mean zonal flow, $\{K'\cdot\overline{K}\}$, is positive when large values of $\overline{u}$ are correlated with latitudinal convergence of the mean eddy momentum transport, $\overline{u'v'}$.

The loss of kinetic energy by lateral eddy-viscosity, $\{\overline{K}\cdot A\}$ and $\{K'\cdot A\}$, is of the same form as that for an incompressible viscous fluid (Lamb 1932). The loss of potential energy by lateral eddy diffusivity, $\{\overline{P}\cdot A\}$ and $\{P'\cdot A\}$, represents the tendency of the diffusion process to smoothe out the temperature gradients. Finally, we note that the loss of kinetic energy by skin friction, $\{\overline{K}\cdot k\}$ and $\{K'\cdot k\}$, can also be written in the form $-k\int\psi_3\zeta_4\,d\sigma$. As Charney and Eliassen have shown (1949), this can be interpreted

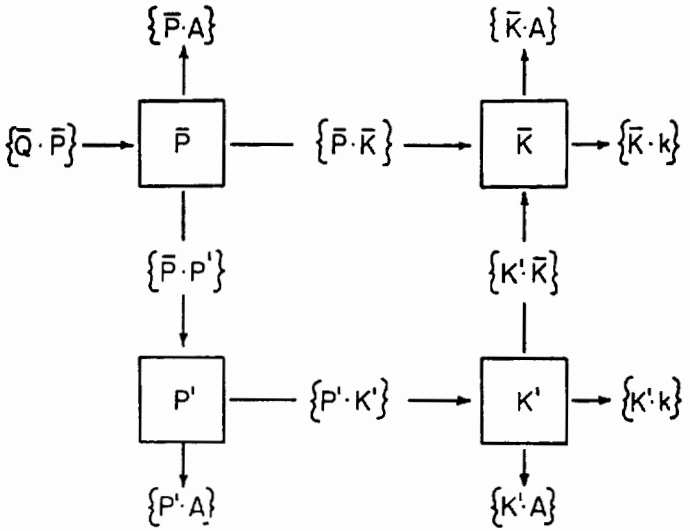

Figure 3. Energy flow diagram. The flow of energy is in the direction of the arrow if the associated transformation $\{\cdot\}$ is positive. The numerical computations give positive values for all the transformations except $\{\bar{P}\cdot\bar{K}\}$.

as an implied reaction of the air above the friction layer to frictionally produced convergence and divergence in the friction layer; the reaction producing horizontal divergence aloft above surface lows and convergence aloft above surface highs. If the flow patterns do not change phase drastically with height, this means a net flow aloft from low to high pressure, with a consequent loss of kinetic energy at those levels.

An interesting way of considering these various energy transformations now is in the form of an energy flow diagram. In this diagram (Fig. 3) each of the four boxes represents a type of energy. The bracketed quantities then represent the 'flow' of energy, their form being given by the above expressions. (The arrows are drawn as if the transformation integrals were all positive – so far merely a matter of definition.)

In a steady state the energy level in each of the boxes must be fixed, and the 'flow' into and out of each box must add up to zero. The old classical theories of the general circulation, since they disregarded the effect of the large eddies in maintaining the mean motion, would imply that the transformation $\{\bar{P}\cdot\bar{K}\}$ is positive, supplying sufficient energy to maintain $\bar{K}$ against friction. This would be accomplished by a direct meridional circulation, $\bar{\omega}_2$ being negative at high temperatures (low latitudes) and positive at low temperatures (high latitudes).

However, the available wind statistics suggest that $\{\bar{P}\cdot\bar{K}\}$ is actually slightly negative (Starr 1954). Since the only other source of energy in our scheme for $\bar{K}$ is K', measurements of $\{K'\cdot\bar{K}\}$ are of great importance in deciding the path of the energy flow. Observations show that $\{K'\cdot\bar{K}\}$ is positive and sufficiently large to account for the frictional losses of $\bar{K}$ (Arakawa 1953, Starr 1953). (Note, however, that in a more complete formulation, $\{K'\cdot\bar{K}\}$ would also include a term $\int\bar{u}\,\partial\,(\overline{u'\omega'})/\partial p\,d\sigma$.) If K' loses energy by $\{K'\cdot\bar{K}\}$, it must therefore gain energy from P', i.e., *as we progress along a latitude circle*, there must be a tendency for cold air to sink and warm air to rise. The difficulty of observing vertical motion, however, has so far prevented any objective measurement of this process.

Finally, if P' is to supply energy to K', it must receive energy from $\overline{P}$ by the transformation $\{\overline{P} \cdot P'\}$. No actual measurements of this have yet been made, although it is easy to see that it must be positive. Examining the integrand in the formula for $\{\overline{P} \cdot P'\}$ in Eq. (44), we note that the first term, $\overline{v_1'(\psi_1' - \psi_3')}$, is proportional to the poleward transport of sensible heat by eddies, and is known to be positive (Fig. 2). The second term, $\partial(\overline{\psi}_1 - \overline{\psi}_3)/\partial y$ is proportional to $\partial \overline{T}_2/\partial y$ and is therefore negative. This, together with the negative sign in front of the integral, shows that $\{\overline{P} \cdot P'\}$ is positive.

The scheme of energy transformations pictured in Fig. 3 (except for the questionable direction of $\{\overline{P} \cdot \overline{K}\}$) thus seems to be a plausible one, in so far as it agrees with what is known at present from observations. It is by no means a new concept, being implicit in most recent writings on the general circulation (e.g. van Mieghem 1952), and has also been independently formulated in the same manner by Lorentz (1955). However, it provides an excellent means for examining the extent to which our simple model contains the physical processes known to be important in the real atmosphere.

The meridional circulation in our model is calculated from the continuity Eq. (3) with the boundary conditions Eq. (5) on ω. Defining the mean meridional velocities, $\overline{V}_1$ and $\overline{V}_3$, by

$$\overline{V}_1 = \frac{1}{Lp_2} \int_0^{p_2} dp \int_0^L v \, dx, \quad . \quad . \quad . \quad . \quad (45)$$

and

$$\overline{V}_3 = \frac{1}{Lp_2} \int_{p_2}^{p_4} dp \int_0^L v \, dx, \quad . \quad . \quad . \quad . \quad (46)$$

we find by integration of Eq. (3) that

$$\frac{\partial \overline{V}_1}{\partial y} = -\frac{\partial \overline{V}_3}{\partial y} = -\frac{\overline{\omega}_2}{p_2}. \quad . \quad . \quad . \quad . \quad (47)$$

$\overline{\omega}_2/p_2$ can then be evaluated either from Eqs. (33), (34), or (35), if ψ_1 and ψ_3 and their time derivatives are known.

We naturally take $\overline{V}_1$ and $\overline{V}_3$ to be equal to zero at $y = -W$. It is then simple to show that the form of Eqs. (17), (18) and (19) is such that $\int_{-W}^{W} \overline{\omega}_2 \, dy$ vanishes, so that $\overline{V}_1$ and $\overline{V}_3$ will also vanish at $y = W$. Since $\overline{V}_1 \equiv -\overline{V}_3$, we need then fix our attention on only $\overline{V}_1$, $\overline{V}_3$ always being the negative of $\overline{V}_1$.

The meridional circulation $\overline{V}$ appears (implicitly) only in the divergence term in the vorticity equation Eqs. (17) and (18) (or Eqs. (33) and (34)), since the remaining terms, e.g., $\mathbf{V} \cdot \nabla\zeta$, were evaluated geostrophically. We must therefore expect that the motions we find in our quasi-geostrophic model, although they contain an implicit mean meridional circulation, do not include the possibility of gravitational-inertia instability of the Høiland-Solberg type (Høiland 1939). That type of instability would, in fact, be retained only if we replaced f_0 by $f + \zeta$ in the divergence term, and also included the non-geostrophic velocities together with the omitted terms $\omega \, \partial u/\partial p$ and $\omega \, \partial v/\partial p$.

By introducing the geostrophic approximation only for the zonal velocity $\bar{u}$, Eliassen (1952) has derived equations for an axially symmetric vortex which to some extent recognize these effects. However, it does not seem possible to retain this feature in a completely quasi-geostrophic model and still keep the internal consistency of Eqs. (17)-(19). The $\overline{V}$ calculated from our model will therefore be only partially applicable to the atmosphere in regions of very large horizontal gradients in $\overline{T}$ and $\bar{u}$ or in equatorial latitudes where f is small.

From the averaged forms Eqs. (33)-(35) of the equations, it is clear that the meridional circulation in a hypothetical steady state depends not only on the 'external' factors of heat and skin friction, but also on the distribution of $\overline{\mathbf{V}' \cdot \nabla\zeta'}$ and $\overline{\mathbf{V}' \cdot \nabla T'}$. As mentioned earlier in the introduction, the latter quantities are observed to be of the same order of magnitude as the former ones, at least in extratropical latitudes, and must be considered just as much as the 'external' factors in any discussion of a mean meridional circulation.

5. Final design of the experiment

A deduction of the atmospheric general circulation from physical principles seems to be most satisfying if it begins with a resting atmosphere, and then demonstrates how the observed motions appear as a natural consequence of the laws of physics. We will follow this approach to some extent, the physical laws in our case being represented by the equations for our simplified quasi-geostrophic model. They are admittedly based on a judicious mixture of empirical fact with physical theory, and therefore have only limited application, but, as we shall see, they go surprisingly far toward providing a partial explanation of the gross features of the general circulation.

The ideal form of our numerical experiment would therefore be to start with an atmosphere at rest, except for some small irregular motions, and simply make a numerical forecast for a long time. At first the latitudinal heating and cooling will begin to create a mean latitudinal temperature gradient. After this has reached a certain critical value, large-scale eddies will presumably develop, having a certain characteristic wavelength (Eady 1949), and modifying the mean zonal flow in turn by non-linear interactions. One would hope that ultimately some sort of quasi-steady state would be reached, in which the input of energy would be balanced by frictional losses, and the typical flow patterns would have some resemblance to those in the actual atmosphere.

By means of linearized perturbation theory, it is possible to estimate both the intensity of the latitudinal temperature gradient which must exist before the initial small irregular motions will begin to amplify, and the dimensions of the dominant wave which will appear. If W is taken as 5,000 km (so that the total 'latitudinal' extent of our region from $y = -W$ to $y = W$ is approximately equal to the equator-to-pole distance on the surface of the earth), one finds that in the two-level model the critical temperature difference between $y = W$ and $y = -W$ is about 56°C, and the most unstable wavelength is about 6,000 km (Phillips 1954).

These values are somewhat unrealistic when compared with the yearly mean temperature difference in the troposphere from pole to equator (about 34°C at 500 mb) and the predominant wavelength of actual extratropical disturbances. The discrepancy seems most likely to be a partial failure of the two-layer model to represent accurately the degree of baroclinic instability in the atmosphere. This has been shown theoretically by Kuo (1953), and is also suggested by differences in numerical forecasts obtained with two- and three-level geostrophic models (Charney 1954). Further calculations with more sophisticated equations will presumably eliminate this difficulty; for the present, however, we can merely recognize its existence.

The size of the electronic computer available for the computations determines the maximum number of grid points we can use to describe the motion in our rectangular region $-W \leqslant y \leqslant W$, $0 \leqslant x \leqslant L$. The computer used was that at the Institute for Advanced Study. It had an 'internal' rapid-access memory of 1024 40-binary digit 'words,' together with a magnetic drum (of slower access time) with a capacity of 2048 such words. Much of this space must be used for the code, however, and this, together with various other considerations (for example, partial duplication of stored information

so as to allow rapid recovery after recognized errors) resulted in a choice of a 17×16 lattice of grid points, 17 in the y-direction, and 16 in the x-direction. Δy was set equal to 625 km, so that the distance $2W$ was equal to 10,000 km. A large value for Δx would presumably allow several eddies to form in the distance $L = 16\Delta x$, but would produce relatively large truncation errors. A smaller value of Δx, on the other hand, would result in the formation of only one large eddy, of wavelength L, but with less truncation error. The latter alternative was taken. Setting L equal to 6,000 km then gave a Δx of 375 km.

In the absence of eddies, the rate of heating we have chosen, Eq. (14), results in a rate of heating and cooling at $y = \pm W$ of about $\pm 0{\cdot}23$°C per day, so that about four months are necessary to create a latitudinal temperature gradient strong enough to give rise to unstable waves. (This is slower than the equivalent mean radiative effects in the actual atmosphere because of the allowances made for latent heat transport and the difference in geometry.) To save time, therefore, a forecast for 130 days was first made with the motion independent of x, i.e. no eddies. This could be done with time steps of one day without violating the computational stability criterion, and resulted in the distributions of mean temperature anomaly and zonal wind shown in Table 1. At this point a small random disturbance ψ' was introduced, varying with x and y but identical at both levels. The forecast from then on was made with the complete equations using time steps of two hours or less, as determined by the computation stability criterion. The initial ψ' values at successive grid points were generated by a random number generating process based on repeated squaring of an initially given generating number. (A discussion of this method is given in ' Monte Carlo Method ', *Appl. Math. Series*, **12**, Nat. Bur. Standards, Washington.)

TABLE 1. DISTRIBUTION OF $\overline{T}_2$, $\bar{u}$, $\overline{V}_1$, AND $\bar{\zeta}_1$ AT THE END OF THE PRELIMINARY FORECAST WITHOUT EDDIES

j	$\overline{T}_2$ (°C)	$\bar{u}_1$ (m sec^{-1})	$\bar{u}_2$ (m sec^{-1})	$\bar{u}_4$ (m sec)$^{-1}$	$\overline{V}_1$ (mm sec^{-1})	$\bar{\zeta}_1$ (10^{-4} sec^{-1})
15	− 30·1	6·1	4·0	− 0·3	11	0·184
14	− 28·2	16·9	11·0	− 0·6	25	0·152
13	− 25·0	24·9	16·3	− 0·9	30	0·104
12	− 20·8	30·1	19·8	− 1·0	28	0·064
11	− 15·9	33·3	21·8	− 1·0	27	0·038
10	− 10·8	35·1	23·0	− 1·1	29	0·020
9	− 5·4	36·0	23·6	− 1·1	28	0·008
8	0	36·3	23·8	− 1·1	29	0
7	5·4	36·0	23·6	− 1·1	28	− 0·008
6	10·8	35·1	23·0	− 1·1	29	− 0·020
5	15·9	33·3	21·8	− 1·0	27	− 0·038
4	20·8	30·1	19·8	− 1·0	28	− 0·064
3	25·0	24·9	16·3	− 0·9	30	− 0·104
2	28·2	16·9	11·0	− 0·6	25	− 0·152
1	30·1	6·1	4·0	− 0·3	11	− 0·184

During the numerical forecasts with the complete equations, a record of the flow patterns was obtained periodically at intervals of one day, so that the development of the motion could be examined in detail. By recording at these times the ψ values at two successive time steps, ω_2 could be computed from Eq. (19), making it possible to calculate all of the different energy transformations, Eq. (44), and the meridional circulation, Eq. (47), every 24 hr. The results are described in the following sections.

6. Development of zonal flow in the absence of eddies

Before discussing the results of the complete forecast containing the eddies, we will examine briefly the results of the preliminary forecast which was made without allowing the motions to vary with x. As mentioned in the previous section, this forecast was made merely to save time, since the large-scale eddies in the two-level model cannot develop until a suitable mean temperature gradient exists.

This forecast started with the 'atmosphere' at rest, i.e. ψ_1 and ψ_3 were identically equal to zero. The heating then caused $\bar{q}_1$ and $\bar{q}_3$ to change according to Eqs. (24) and (25), producing the changes in $\overline{\psi}_1$ and $\overline{\psi}_3$ prescribed by Eqs. (22) and (23). After $\overline{\psi}$ and $\bar{q}$ were no longer identically zero, the motion was affected by the frictional terms $A\,\partial^2\bar{q}/\partial y^2$ and $-k\,\bar{\zeta}_4$ in addition to the heating.

The distribution of mean temperature, $\overline{T}_2$, zonal velocity $\bar{u}$ and the mean meridional circulation, $\overline{V}_1$, at the end (130 days) of this preliminary forecast is shown in Table 1. Here j, the latitudinal coordinate, is equal to $8\,(y + W)/W$. The temperature distribution is very simple, consisting of an almost linear temperature increase from $-30{\cdot}1$°C at $y = W$ to $+30{\cdot}1$°C at $y = -W$. The zonal wind distribution is also very regular, consisting of a very broad west wind at level 1, with a maximum velocity of 36 m sec^{-1}, and uniform weak easterlies everywhere at the ground. As might be expected, the meridional circulation $\overline{V}$ consists of a single weak direct cell, with a maximum velocity of 3 cm sec^{-1}. The mean zonal momentum of the atmosphere [as indicated by the values for $\bar{u}_2 \equiv \frac{1}{2}(\bar{u}_1 + \bar{u}_3)$] is positive, the result of surface friction acting on the weak surface easterlies.

A forecast of this type (no variation with x) using more exact equations (e.g. including the advection of relative zonal momentum $\bar{u}$ by $\overline{V}$) would probably have resulted in weak surface westerlies in high latitudes. Therefore, as has been said earlier in section 3, the meaned form of our present equations furnishes only an incomplete description of the processes in a true Hadley-type circulation, and the results shown in Table 1 cannot be interpreted as a complete picture of that type of circulation. They were obtained only to get an initial zonal wind field to use in making a forecast with the large-scale eddies present.

The zonal kinetic energy $\overline{K}$ and the mean potential energy $\overline{P}$ at the end of the preliminary forecast are given in Table 2, together with the values of the five energy transformation functions associated with the mean flow at that time. The units of $\overline{K}$ are such that a velocity of 1 m sec^{-1} at both level 1 and 3 at every grid point would correspond to a value of 10 for $\overline{K}$. $\overline{P}$ is in the same units. The units for the energy transformations are such that one unit of them corresponds to a change of one unit in $\overline{K}$ (or $\overline{P}$) in 24 hr.

TABLE 2. Energy parameters at end of preliminary forecast

$\overline{K}$	4265
$\overline{P}$	24368
$\{\overline{Q}\cdot\overline{P}\}$	440
$\{\overline{P}\cdot\overline{K}\}$	41
$\{\overline{K}\cdot A\}$	9
$\{\overline{K}\cdot k\}$	−27
$\{\overline{P}\cdot A\}$	48

The energy-transformation functions show that energy in this process is going from $\bar{P}$ to $\bar{K}$, through the agency of the small direct meridional circulation. The *negative* value of $\{\bar{K} \cdot k\}$, signifying an *increase* of zonal kinetic energy at levels 1 and 3 because of skin friction at the ground, is somewhat surprising at first. It is negative because the weak surface easterlies give rise to an (implicit) equatorward flow in the friction layer, which must be balanced by a net poleward flow aloft. Since the mean zonal wind above the friction layer is westerly, this increases the kinetic energy at those levels. We shall see later that as the surface zonal wind distribution becomes more realistic, $\{\bar{K} \cdot k\}$ does become positive.

Before passing on to more interesting results, we note that the jet-like character of the actual atmospheric zonal wind is not present in $\bar{u}_1$ in Table 1. The mean relative vorticity $\bar{\zeta}_1 = -\partial \bar{u}_1/\partial y$ is completely monotonic in character, without the maximum and minimum to the north and south of the maximum value of $\bar{u}$ that is characteristic of a true jet.

7. Development of the flow with eddies present

Following the completion of the preliminary forecast, during which the motion was independent of x, an initial flow pattern was defined by adding a small 'random' disturbance to the mean flow existing at the end of the preliminary forecast. This initial disturbance had a kinetic energy value, K', of 768 units, corresponding to a root mean square velocity of 8·8 m sec^{-1}. Since it was identical at level 1 and 3 $[\psi_1'(x, y, 0) \equiv \psi_3'(x, y, 0)]$, P' was initially zero.

The development of this composite flow pattern with time was then forecast with the complete Eqs. (22)-(25) (including the heating) as described in the appendix. In discussing the results, which in general were obtained at intervals of one day, we shall find it convenient to refer to the results for '3 days,' '18 days,' etc., with '0 days' referring to the time at which the variation with x was introduced.

Table 7 contains a listing of the energy parameters at daily intervals from 0 to 31 days, using the same units as those in Table 2. Looking first at the successive values of K' we see that, following an initial decrease during the first five days, K' showed a steady increase up to 25 days (except for a temporary decrease from 13 to 16 days). After 25 days, the changes in K' are at first irregular and then show a very pronounced increase with time from 28 to 31 days. (These latter changes are highly influenced by truncation errors, and are discussed separately in section 9).

The initial decrease in K' was due to small-scale lateral eddy-viscosity and surface skin friction, as shown by the relatively large initial values for $\{K' \cdot A\}$ and $\{K' \cdot k\}$. The former process was important because of the highly irregular nature of the initial ψ' distribution, while the latter effect was large because ψ_1' and ψ_3' were initially identical (so that the Charney-Eliassen frictional mechanism was very efficient).

During the period from five days to about 23-27 days, a very regular wave developed having many of the features of the large-scale eddies seen on actual weather charts. Figs. 4 to 9 contain the 1,000-mb flow pattern (defined by $\psi_4 = \frac{3}{2}\psi_3 - \frac{1}{2}\psi_1$) and the 500-mb temperature pattern (proportional to the values of $\psi_1 - \psi_3$) at intervals of three days during part of this period. The following points may be noted :

(a) The wave moves eastward at a speed of about 1,800 km/day, the apparent slow westward motion on the charts appearing only because they are shown at three-day intervals. The regularity of this, as well as that of other features present in the figures, is borne out by the intermediate charts which are not shown.

(b) The wave begins as a 'warm low' (e.g., at eleven days), but the tongue of cold air gradually catches up with the deepening surface low centre, and the tongue of warm

air moves over the surface high centre, so that the final stages (e.g. 23 and 26 days) look very much like those of an *occluded cyclone*.

(c) The main surface troughs and ridges (and also those at the upper levels) are orientated so as to lean back towards the north-west in the northern half of the region, and toward the south-west in the southern half of the region.

(d) Definite indications of something similar to cold and warm fronts are to be seen in the 1,000-mb contours, with the main temperature gradient occurring on the cold side of the ' frontal ' troughs. On some charts (e.g. 17 days) these are so pronounced

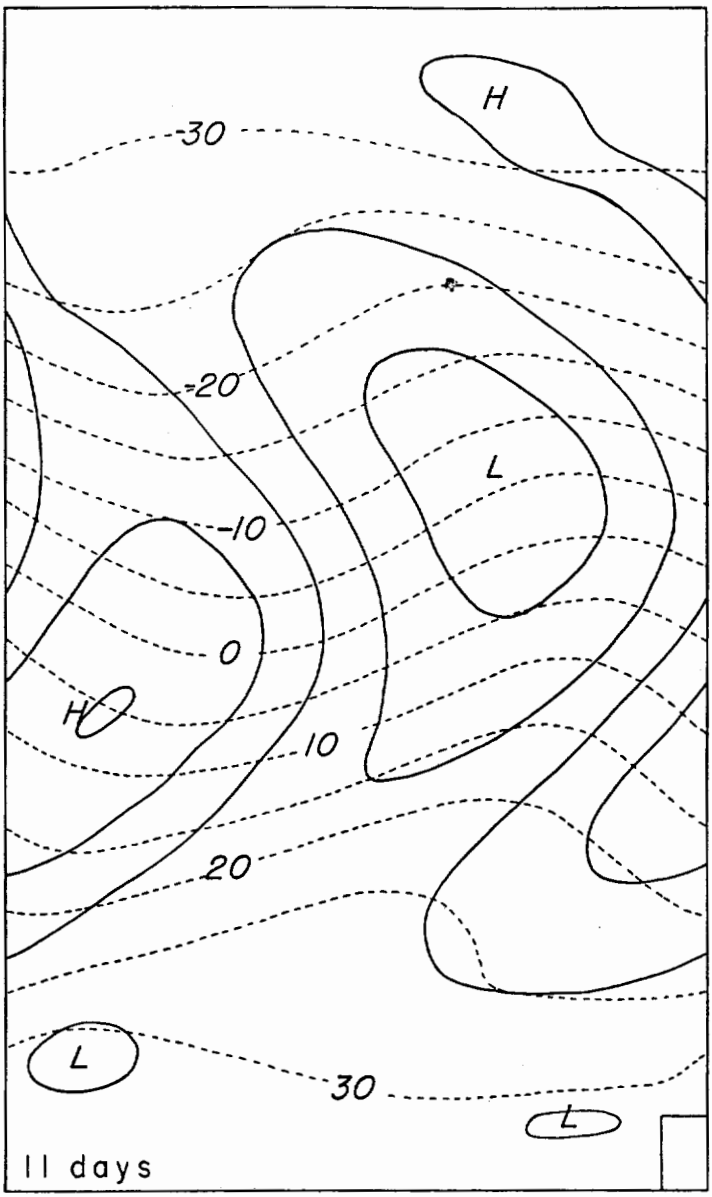

Figure 4. Distribution of 1,000-mb contour height at 200-foot intervals (solid lines) and 500-mb temperature at 5°C intervals (dashed lines) at 11 days. The small rectangle in the lower right corner shows the size of the finite-difference grid intervals Δx and Δy.

as almost to force a kinking of the contour lines. (Because of the symmetry of the equations, equally sharp ridges are also formed. This symmetry would be removed if $f + \zeta$ replaced f_0 as the coefficient of the horizontal divergence in the vorticity equation).

The field of vertical motion at 500 mb at 20 days is shown in Fig. 10. Here the vertical velocities w_2 were obtained from ω_2, using the relationship $w_2 \simeq -\omega_2 (z_1 - z_3)/p_2$ The overall aspect is quite realistic, especially the rapid changes from ascending to descending motion in the vicinity of the frontal troughs, together with the general ascent

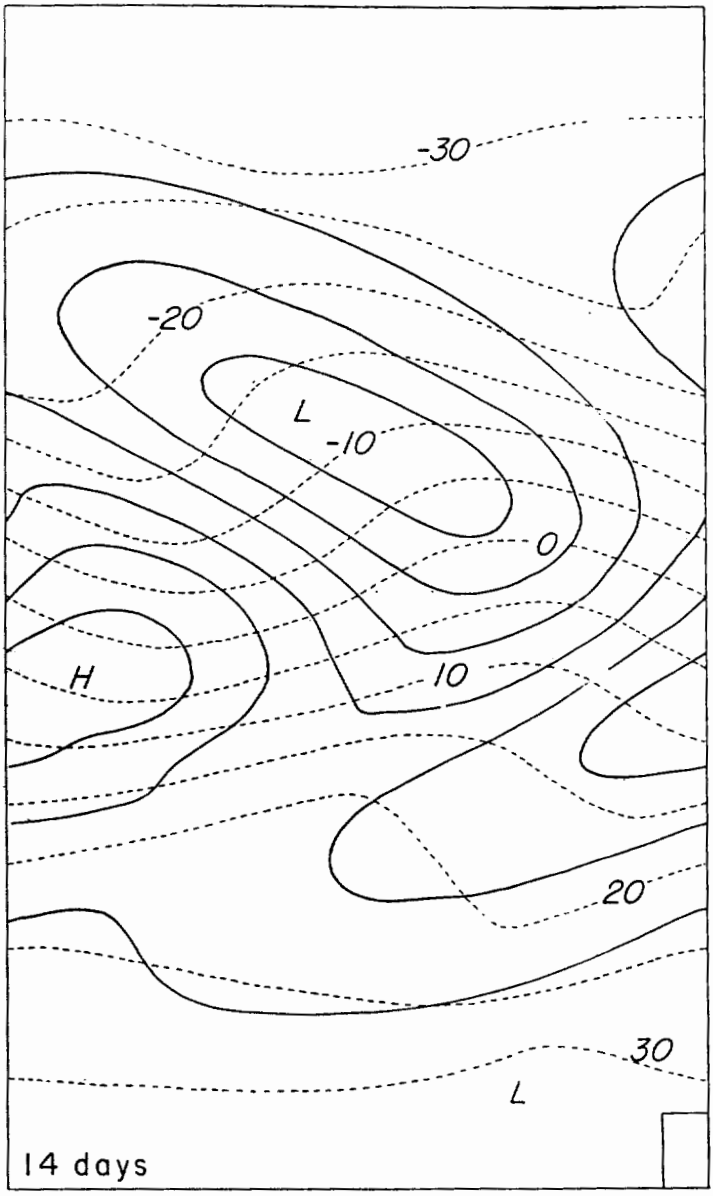

Figure 5. Distribution of 1,000-mb contour height at 200-foot intervals (solid lines) and 500-mb temperature at 5°C intervals (dashed lines) at 14 days. The small rectangle in the lower right corner shows the size of the finite-difference grid intervals Δx and Δy.

in the region of the main low and the descent associated with the high pressure centre.

In Fig. 11 the meridional circulation $\overline{V}_1$ is shown. According to Eq. (45), this is the mean meridional motion in the upper half of the atmosphere, the circulation in the lower half being equal and opposite. Initially we find only the very weak and broad direct cell characteristic of the preliminary forecast without eddies. As the eddy develops, however, we see the appearance of a definite three-celled circulation, with an indirect cell in middle latitudes and two somewhat weaker direct cells to the north and south. This is a characteristic feature of the unstable baroclinic waves in the two-level model, as has

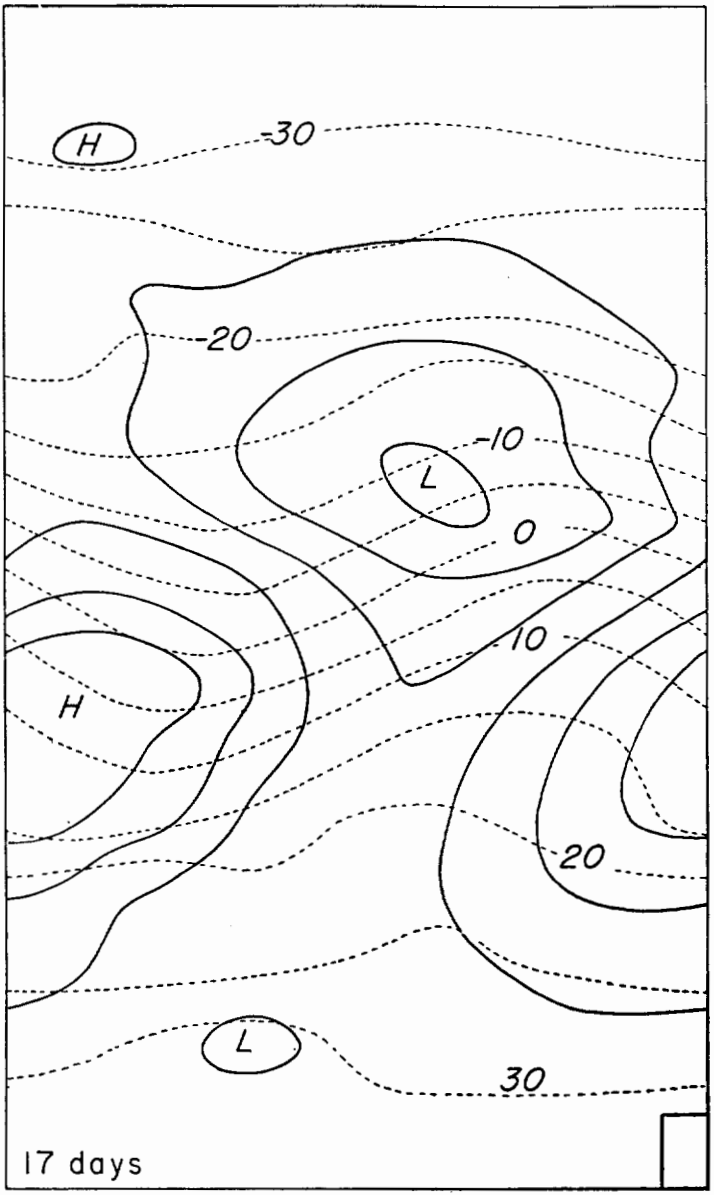

Figure 6. Distribution of 1,000-mb contour height at 200-foot intervals (solid lines) and 500-mb temperature at 5°C intervals (dashed lines) at 17 days. The small rectangle in the lower right corner shows the size of the finite-difference grid intervals Δx and Δy.

been shown previously by the writer (Phillips 1954). After 26 days, the field of $\overline{V}$ became very irregular owing to large truncation errors, and is therefore not shown.

The variation with time of the mean temperature at 500 mb, $\overline{T}_2$, is illustrated in Fig. 12, in the form of the accumulated temperature change since zero days. In the first five days, the temperature difference between $y = -W (j = 0)$ and $y = W (j = 16)$ continued to increase at the same rate (about 0·4°C per day) as that which prevailed during the preliminary forecast without eddies. As the disturbance developed, it transported sensible heat poleward because of the correlation between v' and T_2' (Figs. 4-9). This

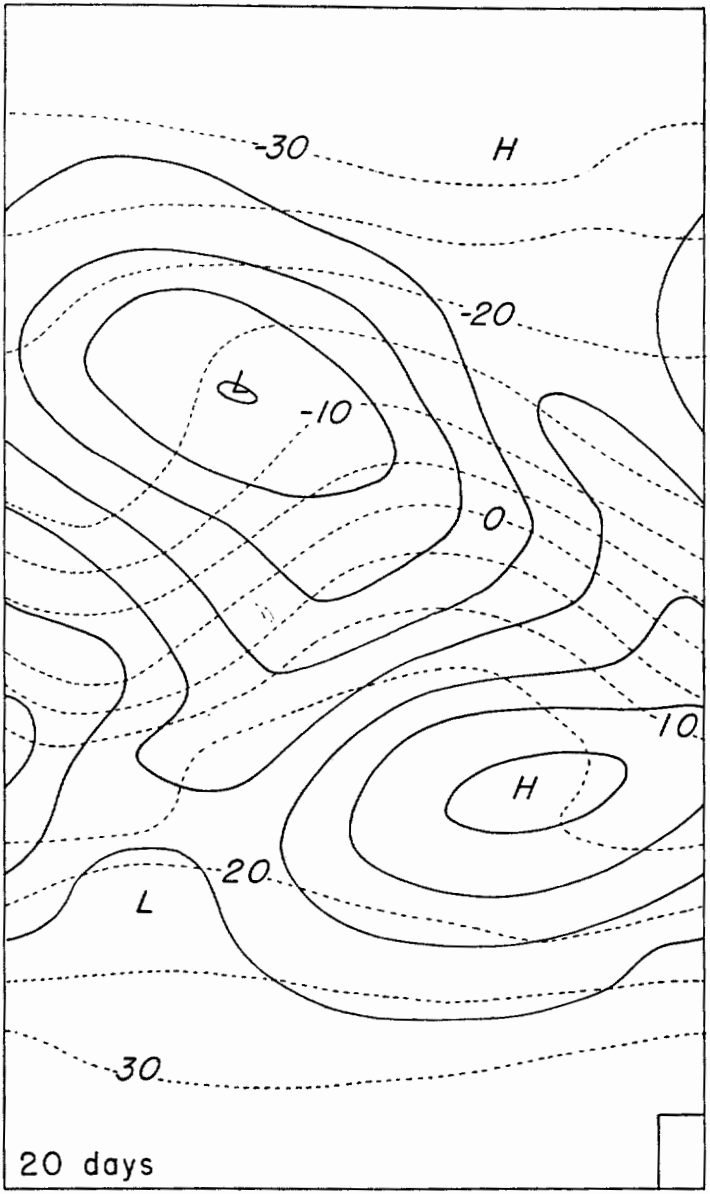

Figure 7. Distribution of 1,000-mb contour height at 200-foot intervals (solid lines) and 500-mb temperature at 5°C intervals (dashed lines) at 20 days. The small rectangle in the lower right corner shows the size of the finite-difference grid intervals Δx and Δy.

stopped the increase in the total mean temperature difference and eventually reduced it at the end of the period to a value below that existing at 0 days. In the later stages of the process (23-28 days) we find a marked concentration of the temperature gradient in central latitudes, while to the north and south the temperature gradient is very weak. By this time the exchange process had produced a relatively warm region at $j = 13$ and a relatively cool region at $j = 3$, reminiscent of the cut-off warm highs and cold lows frequently observed to the north and south of the main westerly current on actual atmospheric charts (Fig. 9).

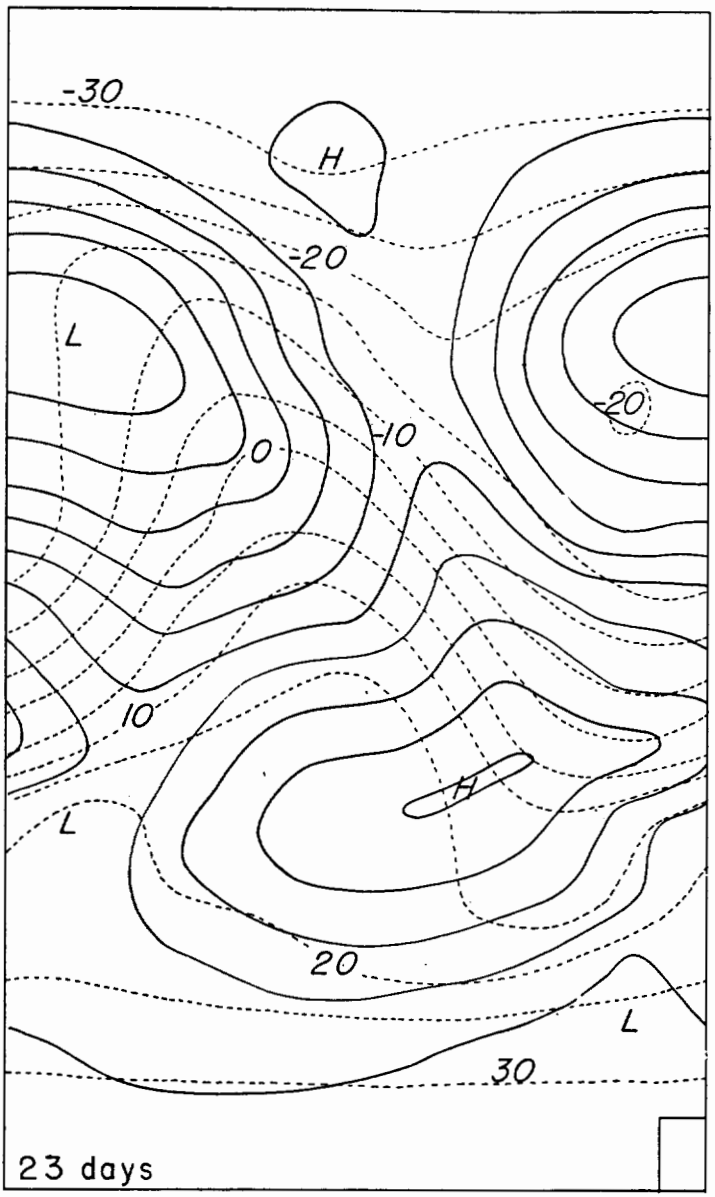

Figure 8. Distribution of 1,000-mb contour height at 200-foot intervals (solid lines) and 500-mb temperature at 5°C intervals (dashed lines) at 23 days. The small rectangle in the lower right corner shows the size of the finite-difference grid intervals Δx and Δy.

The thermodynamic energy equation for the model, Eq. (19), can be written in its x-averaged form as

$$\frac{\partial \bar{T}_2}{\partial t} = -\frac{\partial \overline{v_1' T_2'}}{\partial y} - \frac{2H}{c_p}\frac{y}{W} + \frac{f_0^2}{R\lambda^2 p_2}\bar{\omega}_2 + A\frac{\partial^2 \bar{T}_2}{\partial y^2}. \quad . \quad . \quad . \quad (48)$$

The average size and distribution with y of the five terms in this equation during the period 10-20 days are show in Table 3, with $y = (j - 8)\,\Delta y$. The contribution from the non-adiabatic heating, given by $-2Hy/c_pW$, is of course a warming at low latitudes

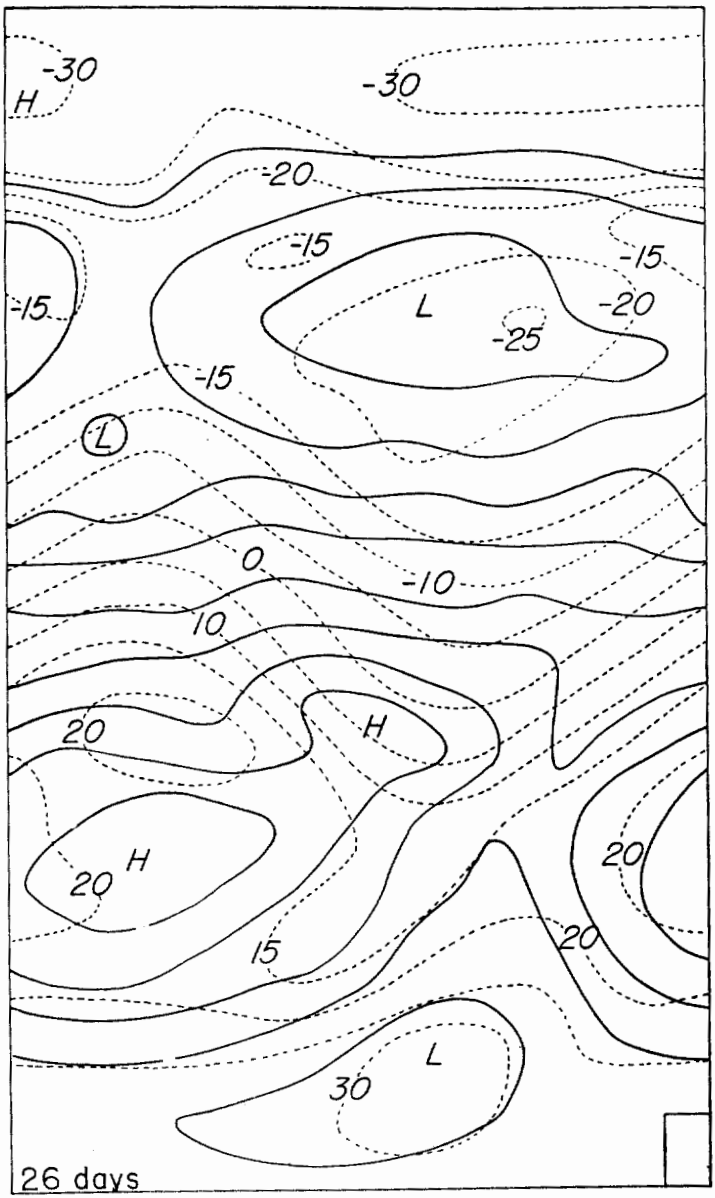

Figure 9. Distribution of 1,000-mb contour height at 200-foot intervals (solid lines) and 500-mb temperature at 5°C intervals (dashed lines) at 26 days. The small rectangle in the lower right corner shows the size of the finite-difference grid intervals Δx and Δy.

($j < 8$) and a cooling at high latitudes ($j > 8$). The convergence of the eddy transport $-\partial(\overline{v_1' T_2'})/\partial y$ opposes this, tending to destroy the latitudinal temperature gradient, especially in the centre of the region. On the other hand, the temperature change produced by the mean meridional circulation, $(f^2/R\lambda^2 p_2) \cdot \overline{\omega}_2$ cancels the non-adiabatic

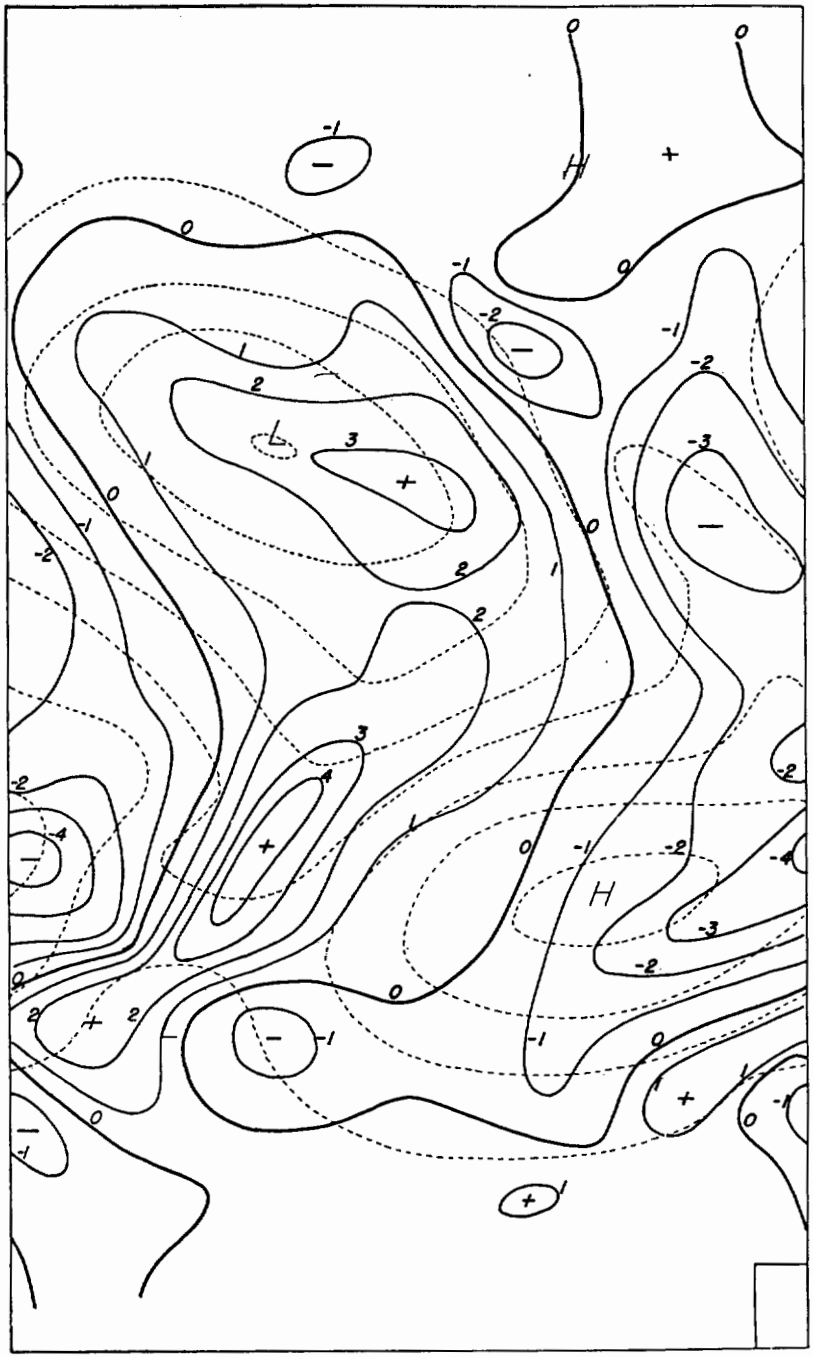

Figure 10. Distribution of vertical velocity at 500 mb in cm sec^{-1} (solid lines) and 1,000-mb contour height at 200-ft intervals (dashed lines) at 20 days. The small rectangle in the lower right corner shows the size of the finite-difference grid intervals Δx and Δy.

effect near the walls, but, because of the indirect circulation in middle latitudes, contributes greatly to an *increase* in $-\partial\overline{T}_2/\partial y$ in the centre of the region. The resulting temperature changes, $\partial\overline{T}_2/\partial t$, show a tendency to a decrease of the temperature gradient in the outer regions, $0 < j < 6$ and $10 < j < 16$, and a tendency towards an increase in the centre $6 < j < 10$. (We note that the contribution from the lateral diffusion is generally negligible.)

Although the numbers in Table 3 do not represent a completely steady state, they

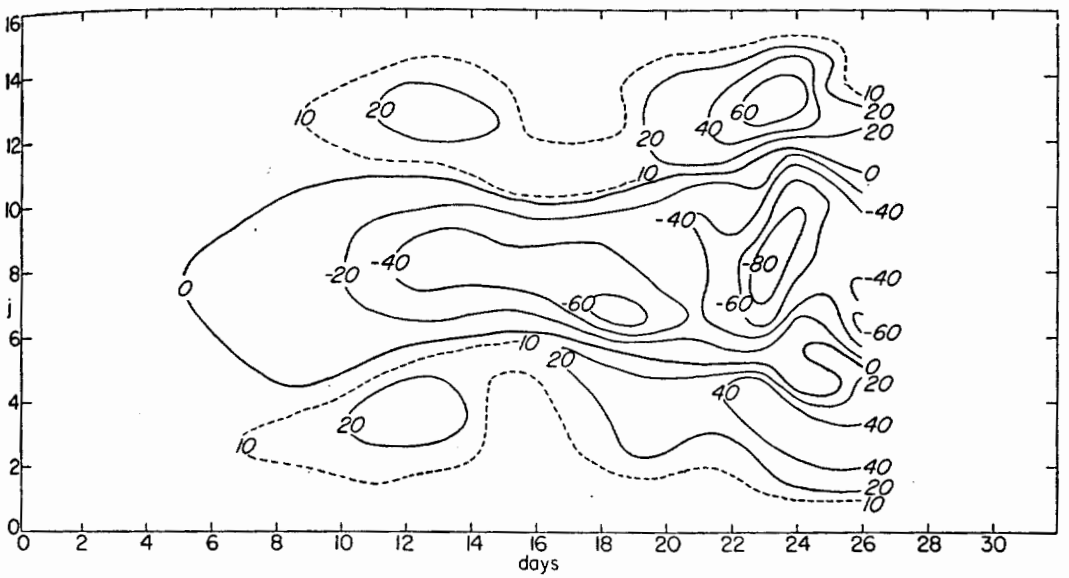

Figure 11. Variation with latitude (j) and time of the mean meridional velocity, $\overline{V}_1$, in the upper half of the atmosphere. Units are cm sec^{-1}.

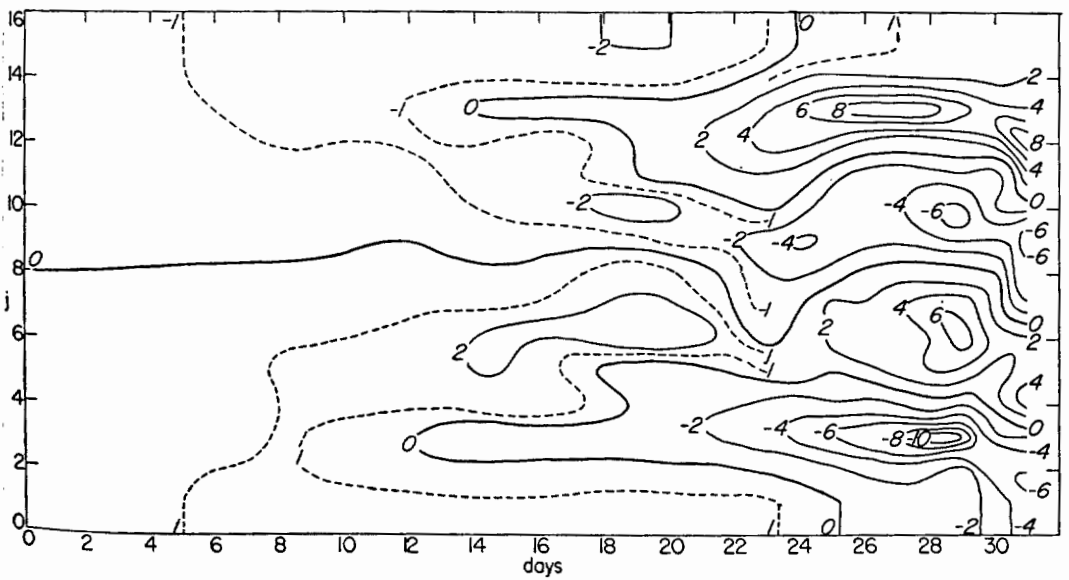

Figure 12. Variation of 500 mb mean temperature, $\overline{T}_2$, with latitude (j) and time, shown as the accumulated change from the temperature distribution at the end of the preliminary forecast (Table 1). Units are °C.

suggest that the latitude of maximum $\partial\overline{T}/\partial y$ in the atmosphere may be determined to some extent dynamically, and not merely by the latitudinal gradient in radiation.

The changes with time of $\bar{u}_1$ and $\bar{u}_4$, the mean zonal velocities at 250 and 1,000 mb, are shown in Figs. 13 and 14. The interesting phenomena here are (*a*) the formation of a strong jet in the centre of the region, and (*b*) the change in $\bar{u}_4$ from uniform weak easterlies to a pattern with westerlies in middle latitudes and easterlies to the north and south. The processes which create these changes can be seen by studying the zonal momentum budgets of the upper and lower halves of the atmosphere.

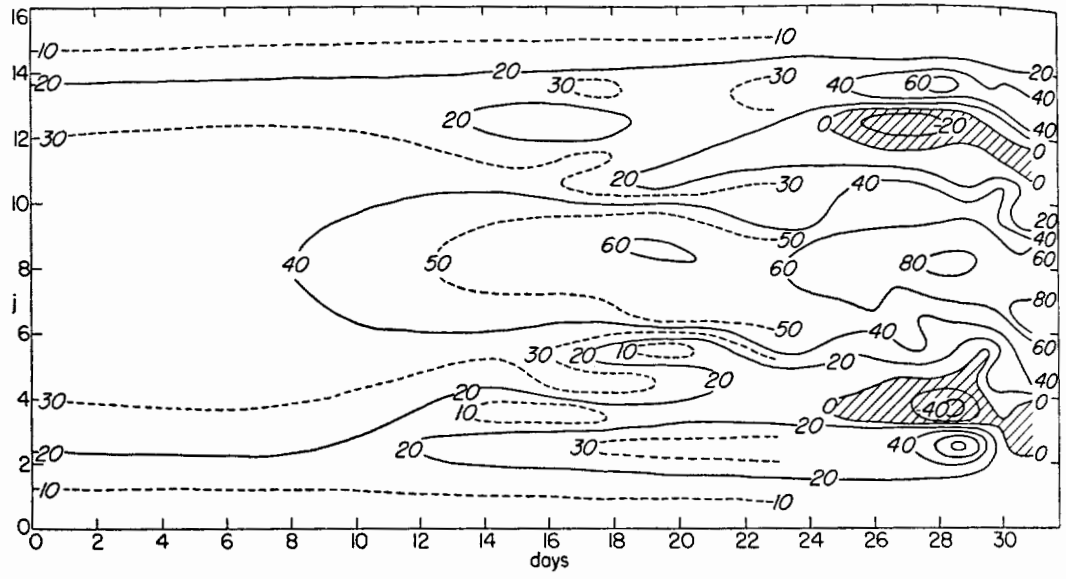

Figure 13. Variation of $\bar{u}_1$, at 250 mbs with latitude (j) and time. Units are m sec^{-1}. Regions of easterly winds are shaded.

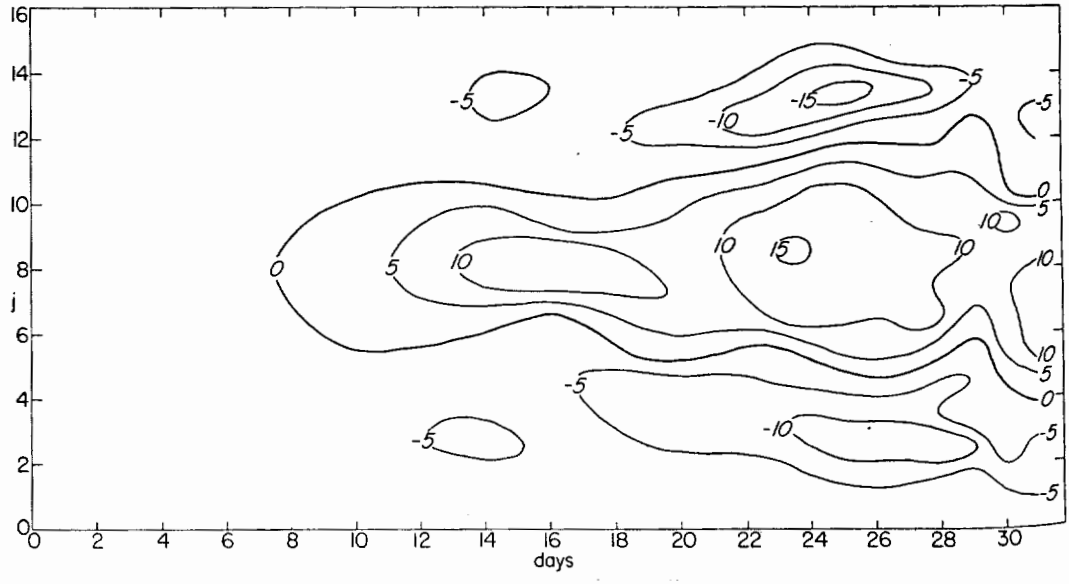

Figure 14. Variation of $\bar{u}_4$, at 1,000 mb with latitude (j) and time. Units are m sec^{-1}.

TABLE 3. EVALUATION OF THE TERMS IN THE THERMODYNAMIC ENERGY EQUATION DURING THE PERIOD 10-20 DAYS. UNITS ARE DEG DAY^{-1}.

j	$\frac{\partial \bar{T}_2}{\partial t}$	$-\frac{2H}{c_p}\frac{y}{W}$	$\frac{f_0^2}{R\lambda^2}\frac{\bar{\omega}_2}{p_2}$	$-\frac{\partial(\overline{v_1' T_2'})}{\partial y}$	$A\frac{\partial^2 \bar{T}_2}{\partial y^2}$
15	− 0·01	− 0·30	0·23	0·01	0·05
14	0·06	− 0·26	0·22	0·06	0·04
13	0·16	− 0·22	0·08	0·32	− 0·02
12	0·21	− 0·17	− 0·08	0·43	0·03
11	0·10	− 0·13	− 0·38	0·61	− 0·00
10	− 0·20	− 0·09	− 0·97	0·82	0·04
9	− 0·10	− 0·04	− 0·36	0·30	0·00
8	0·12	0·00	− 0·05	0·18	− 0·01
7	0·16	0·04	0·39	− 0·28	0·01
6	0·29	0·09	1·16	− 1·01	− 0·05
5	− 0·25	0·13	0·29	− 0·69	0·02
4	− 0·22	0·17	0·08	− 0·41	− 0·06
3	− 0·26	0·22	− 0·14	− 0·39	0·05
2	− 0·05	0·26	− 0·22	− 0·05	− 0·04
1	0·00	0·30	− 0·25	0·01	− 0·06

From Eq. (1) in its averaged form, we find that the change in $\bar{u}_1$ with time is given by

$$\partial \bar{u}_1/\partial t = -\partial(\overline{u_1' v_1'})/\partial y + f_0 \bar{V}_1 + A\,\partial^2 \bar{u}_1/\partial y^2 . \quad . \quad . \quad (49)$$

(This equation may also be obtained by integrating Eq. (33) with respect to y from $y = -W$ to $y = y$.) The values of these four quantities are listed in Table 4 as a function of y (j), averaged over the period 10 days to 20 days. (They are listed at values of j equal to $n + \frac{1}{2}$, because the finite-difference equivalent of Eq. (49) is valid at those points.) The value for $\partial \bar{u}_1/\partial t$ in the table is one-tenth of the difference between $\bar{u}_1$ at 20 days and 10 days. $f_0 \bar{V}_1$ was evaluated from the time mean of $\bar{V}_1$ during this period, using the values calculated every 24 hr from the finite-difference analogues of Eqs. (19) and (45). The term $A\,\partial^2 \bar{u}_1/\partial y^2$ was evaluated by finite differences from the time mean values of $\bar{u}_1$ during the ten days. The large-scale eddy stress term $-\partial(\overline{u_1' v_1'})/\partial y$ was then obtained from the difference in the other terms in Eq. (49).

TABLE 4. MOMENTUM BUDGET FOR THE UPPER HALF OF THE ATMOSPHERE DURING THE PERIOD 10-20 DAYS (Units are m sec^{-1} day^{-1}).

j	$\frac{\partial \bar{u}_1}{\partial t}$	$f_0 \bar{V}_1$	$A\frac{\partial^2 \bar{u}_1}{\partial y^2}$	$-\frac{\partial(\overline{u_1' v_1'})}{\partial y}$
14·5	0·35	0·59	− 0·07	− 0·17
13·5	0·54	1·17	− 0·43	− 0·20
12·5	− 0·26	1·39	0·40	− 2·05
11·5	− 0·93	1·19	− 0·17	− 1·95
10·5	− 1·66	0·16	0·31	− 2·13
9·5	1·29	− 2·43	− 0·27	3·99
8·5	1·82	− 3·40	− 0·16	5·38
7·5	1·12	− 3·54	− 0·04	4·70
6·5	1·73	− 2·48	− 0·31	4·52
5·5	− 3·31	0·65	0·48	− 4·44
4·5	− 0·49	1·42	− 0·45	− 1·46
3·5	− 0·84	1·64	0·69	− 3·17
2·5	1·19	1·26	− 0·55	0·48
1·5	0·34	0·67	− 0·10	− 0·23

During this time the changes in $\bar{u}_1$ – an increase in middle latitudes with decreases to the north and south – are evidently determined mainly by the Coriolis term $f_0 \bar{V}_1$ and the large-scale eddy stress term $-\partial(\overline{u_1' v_1'})/\partial y$, the latter of these two being the larger. The contribution from the meridional circulation is in general opposite to the *observed* changes in $\bar{u}_1$, *so as to reduce the effect of the eddy term at level 1.* The resulting picture in central latitudes is thus very much like that postulated by Rossby as existing during the building up of a zonal wind maximum (Staff members 1947).

The momentum budget for the lower half of the atmosphere may be studied by means of the equation

$$\partial \bar{u}_3/\partial t = -\partial(\overline{u_3' v_3'})/\partial y + f_0 \bar{V}_3 + A\,\partial^2 \bar{u}_3/\partial y^2 - k\,\bar{u}_4 \quad . \quad . \quad (50)$$

Table 5 lists the values of these quantities in a fashion analogous to those in Table 4. Here we find that the principal terms are the Coriolis term $f_0 \bar{V}_3$ and the surface skin-friction term $-k\,\bar{u}_4$, these two being usually of the same magnitude but opposite in sign.

The importance for the zonal momentum balance in our model of the implicit meridional circulation characteristic of the amplifying baroclinic wave is thus quite clear: it tends to balance both the large values of $-\partial(\overline{u' v'})/\partial y$ in the upper atmosphere and the effect of surface friction on the lower atmosphere. The simultaneous development of middle-latitude surface westerlies and a jet is thus a combined result of the large-scale eddy momentum transport $\overline{u' v'}$ and the meridional circulation $\bar{V}$.

The meridional circulation, as is clear from Tables 4 and 5, is such as to *reduce* the large change in zonal wind shear with height, $\partial(\bar{u}_1 - \bar{u}_3)/\partial t$, which would otherwise result from the large-scale eddy-stress terms and skin friction alone. This result has previously been derived by Fjørtoft (1951).

TABLE 5. MOMENTUM BUDGET FOR THE LOWER HALF OF THE TROPOSPHERE DURING THE PERIOD 10-20 DAYS (Units are m sec^{-1} day^{-1}).

j	$\frac{\partial \bar{u}_3}{\partial t}$	$f_0 \bar{V}_3$	$A\frac{\partial^2 \bar{u}_3}{\partial y^2}$	$-\frac{\partial(\overline{u_3' v_3'})}{\partial y}$	$-k\bar{u}_4$
14·5	0·03	− 0·59	− 0·02	− 0·06	0·70
13·5	0·06	− 1·17	− 0·12	− 0·02	1·37
12·5	− 0·46	− 1·39	0·14	− 0·68	1·47
11·5	− 0·46	− 1·19	− 0·02	− 0·53	1·28
10·5	− 0·40	− 0·16	0·12	− 0·46	0·10
9·5	0·75	2·43	− 0·09	− 0·02	− 1·57
8·5	0·88	3·40	− 0·13	0·91	− 3·30
7·5	0·87	3·54	− 0·09	0·48	− 3·06
6·5	1·14	2·48	− 0·06	− 0·33	− 0·95
5·5	− 0·89	− 0·65	0·15	− 0·64	0·25
4·5	− 0·60	− 1·42	− 0·09	− 0·79	1·70
3·5	− 0·68	− 1·64	0·24	− 1·02	1·74
2·5	0·25	− 1·26	− 0·15	0·07	1·59
1·5	0·09	− 0·67	− 0·03	0·00	0·79

Eqs. (49) and (50) are at most only approximate statements of the real atmospheric momentum budget (although they are exact for our simplified model). The same equations for the atmosphere should also include the following additional types of terms on the right side of, say, Eq. (49):

$$-\partial(\bar{u}_3 \bar{V}_3)/\partial y + \bar{\omega}_2 \bar{u}_2/p_2 + \overline{\omega_2' u_2'}/p_2 \quad . \quad . \quad . \quad (51)$$

In order to obtain some idea of the importance of these terms, whose effect is not included in our model, they have been evaluated from the fields of u and ω at 23 days, and are shown in Table 6. (Some ambiguity arises from their finite-difference evaluation because $\bar{u}_3$ and $\overline{V}_3$ are logically measured at values of $j = n + \frac{1}{2}$ while ω is defined at integral values of j. This was resolved by using simple interpolation where necessary.) For comparison, Table 6 also contains the values of $f_0 \overline{V}_3$ and $-k\bar{u}_4$ at 23 days. Each of the three terms in Eq. (51) are as large at *some* latitudes as the surface skin-friction term or the Coriolis term, but in general they are smaller than the latter two. Their sum, it is interesting to note, would act to increase the 'subtropical' surface easterlies and to diminish the 'polar' easterlies. This suggests that a model incorporating these terms might predict this feature of the real zonal circulation at the surface, i.e. that the trade winds are much more pronounced than the polar easterlies. Our simple equations, because of their symmetry, are deficient in this respect.

Implicit in all of these results is the initial assumption that the small-scale vertical stress, τ_x and τ_y, can be neglected at the 500-mb level. If this assumption is not valid, i.e. if τ at that level is an appreciable fraction of the stress at the ground, the computations here must be viewed with some scepticism. For example, Sheppard (1953), in discussing qualitatively the importance for the momentum budget of an appreciable vertical small-scale eddy stress in the free atmosphere, reached quite different conclusions concerning the meridional circulation in middle latitudes. The intensity of the Ferrel-type cell would of course be diminished by a net downward-directed τ at 500 mb, but this stress would have to be comparable with that at the ground before it would alter appreciably the results shown in Table 4. Although there is some recent evidence suggesting that τ does not decrease as rapidly with height as has hitherto been supposed (Sheppard, Charnock and Francis 1952), there is as yet no clear indication that τ at 5 km is very large.

TABLE 6. ADDITIONAL MOMENTUM TERMS FOR THE LOWER HALF OF THE ATMOSPHERE AT 23 DAYS (Units are m sec^{-1} day^{-1}).

j	A $\dfrac{\overline{\omega_2 \bar{u}_2}}{p_2}$	B $-\dfrac{\partial(\bar{u}_3 \overline{V}_3)}{\partial y}$	C $\dfrac{\overline{\omega_2' u_2'}}{p_2}$	Sum of $A+B+C$	$f_0 \overline{V}_3$	$-k\bar{u}_4$
15	0·40	− 0·14	0·06	0·32	− 1·36	0·88
14	1·16	− 0·23	0·06	0·99	− 4·25	2·77
13	− 0·24	0·40	1·49	1·65	− 5·46	4·06
12	− 1·28	− 0·02	3·92	2·62	− 2·33	2·49
11	− 0·48	0·40	1·60	1·52	1·16	− 0·78
10	− 1·37	0·77	1·40	0·80	3·00	− 3·15
9	− 2·70	2·21	0·85	0·36	5·75	− 4·68
8	− 0·73	− 0·03	0·88	0·12	7·69	− 4·80
7	1·78	− 0·84	1·19	2·13	7·15	− 4·04
6	4·37	− 2·28	0·65	2·74	3·70	− 1·57
5	2·27	− 0·13	− 2·82	− 0·68	− 1·81	1·13
4	− 0·04	− 0·02	− 3·17	− 3·23	− 4·57	2·42
3	− 0·68	− 0·39	− 0·78	− 1·85	− 3·42	2·80
2	− 0·59	0·21	0·05	− 0·33	− 1·75	1·70
1	− 0·16	0·08	− 0·00	− 0·08	− 0·56	0·49

8. ENERGY TRANSFORMATIONS DURING THE FORECAST

One of the main purposes of this numerical experiment was the investigation of the energetics of the atmosphere. Table 7 contains values of the various energy parameters obtained during the course of the general forecast at 24-hourly intervals. The units are the same as those given for Table 2 in section 5. We will consider in this section only

the values from about 5 to 26 days, the later values requiring a separate discussion since they contain large truncation errors, and the earlier values being of no special interest. The mean values of the energy parameters during the period 5-26 days are also included in the table.

Looking first at the energy input values, $\{\overline{Q} \cdot \overline{P}\}$, we see that this is uniformly positive, as is to be expected from the positive correlation between the heating and $\overline{T}_2$. The mean value of $\{\overline{Q} \cdot \overline{P}\}$ over the period 5-26 days is 448 units, while the *calculated* dissipation of energy during this period is almost as large, the sum of the 6 dissipation terms being 423 units.

The average $\{\overline{Q} \cdot \overline{P}\}$ value of 448 units corresponds to a rate of energy input of about 2·6 joules $\text{sec}^{-1}\ \text{m}^{-2}$, about half of the estimated rate of energy dissipation in the real atmosphere (Brunt 1944). Although it is possible to assign part of this discrepancy to the smallish value we chose for H (H having been determined so as to get 'similarity' only in the latitudinal eddy transport of sensible heat), the model itself is undoubtedly too simple for us to expect any closer agreement.

In Section 4 a scheme was outlined for the energy transformations occurring in the atmosphere, where the kinetic energy $\overline{K}$ of the zonal motion was maintained by a flow of energy from the eddies, which received their energy in turn from the mean potential energy $\overline{P}$ (see also Lorentz 1955). The mean values of $\{\overline{P} \cdot P'\}$, $\{P' \cdot K'\}$, and $\{K' \cdot \overline{K}\}$ in Table 7 agree with this picture (Fig. 3), all three values being positive.

The direct exchange of energy between $\overline{P}$ and $\overline{K}$, given by $\{\overline{P} \cdot \overline{K}\}$, is predominantly *negative* in Table 7, especially after the appearance of surface westerlies in middle latitudes. This is a result of the greater intensity of the central indirect cell compared to the weaker direct cells to the north and south (Fig. 11), and to the relatively large mean temperature gradient in middle latitudes. However, the magnitude of $\{\overline{P} \cdot \overline{K}\}$ is small, and it is conceivable that a true Hadley-type circulation in low latitudes (for which our present theory is to some extent inadequate) might contribute enough to make $\{\overline{P} \cdot \overline{K}\}$ positive, although it would undoubtedly still be small in comparison to $\{K' \cdot \overline{K}\}$.

The pictorialisation of the direction of the energy transformations in Fig. 3 is thus borne out by the computations, except that $\{\overline{P} \cdot \overline{K}\}$ is negative. It is of course not possible to state definitely that this diagram is a complete representation of the principal energy changes occurring in the atmosphere, since our equations are so simplified, but the verisimilitude of the forecast flow patterns suggests quite strongly that it contains a fair element of truth. Further computations with more exact equations will presumably refine the picture considerably, as will an extension of observational studies using real data.

Of the amount of energy dissipated by friction during the period 5-26 days, somewhat more than half was done through the agency of the lateral eddy-vicosity A, whose value is perhaps one of the least satisfactorily known parameters in the experiment. As a check on the importance of this parameter, the experiment was re-run with $A = 0$. The development of the flow pattern was in general quite similar to that with $A = 10^5\ \text{m}^2\ \text{sec}^{-1}$, except that large truncation errors appeared earlier in the forecast period, so that the check computation with $A = 0$ could not be carried as far as the one containing the lateral viscosity. The direction of the energy transformation was, however, the same.

9. Finite-difference (truncation) errors

An exact detailed analysis of the truncation errors introduced by the employment of finite differences is of course possible only when the continuous solution of the differential equation is known. In our case this is not possible (if it were, there would be no need to use finite differences), and we must therefore use some cruder technique.

TABLE 7. ENERGY AND ENERGY-TRANSFORMATION VALUES

Days	K'	$\overline{K}$	P'	$\overline{P}$	E	$\{\overline{Q}\cdot\overline{P}\}$	$\{\overline{P}\cdot P'\}$	$\{P'\cdot K'\}$	$\{K'\cdot\overline{K}\}$	$\{\overline{P}\cdot\overline{K}\}$	$\{\overline{K}\cdot k\}$	$\{K'\cdot k\}$	$\{\overline{K}\cdot A\}$	$\{K'\cdot A\}$	$\{\overline{P}\cdot A\}$	$\{P'\cdot A\}$
0	768	4265	0	24368	29401	440	0	0	− 11	41	− 27	266	9	330	48	0
1	357	4328	24	24698	29407	443	3	18	− 27	41	− 27	102	9	139	48	8
2	215	4389	20	25044	29668	446	5	4	− 6	41	− 27	26	9	73	49	5
3	161	4450	19	25380	30010	449	20	12	− 7	35	− 28	8	10	45	50	3
4	139	4513	29	25708	30389	452	38	22	− 0	34	− 28	5	10	30	50	2
5	137	4578	46	26016	30777	455	65	44	11	32	− 27	4	10	21	51	2
6	159	4649	68	26300	31176	457	101	80	28	41	− 26	7	10	17	52	3
7	198	4723	94	26554	31569	460	150	132	53	36	− 23	12	10	16	52	3
8	260	4806	130	26756	31952	461	229	203	81	14	− 19	21	10	17	52	4
9	356	4890	182	26873	32301	462	335	306	122	7	− 12	34	10	20	53	6
10	493	4988	251	26891	32623	462	464	431	193	− 28	− 0	49	11	26	53	8
11	678	5113	333	26786	32910	461	614	592	291	− 37	21	67	12	36	53	11
12	867	5279	409	26562	33117	460	719	766	441	− 43	55	84	15	49	52	14
13	968	5530	407	26335	33240	457	636	831	625	− 72	99	92	23	62	53	15
14	909	5770	298	26289	33266	457	411	666	577	− 72	128	84	33	71	53	14
15	813	5848	204	26403	33268	458	313	438	352	− 99	128	61	42	75	54	11
16	795	5819	217	26483	33314	458	433	403	212	− 119	115	45	51	75	55	11
17	875	5826	312	26386	33399	458	646	548	235	− 128	110	50	59	75	55	13
18	1004	5994	419	26125	33542	455	783	719	381	− 192	114	66	75	75	57	16
19	1171	6265	495	25798	33729	452	832	770	324	− 151	125	80	99	77	59	18
20	1542	6278	616	25368	33804	449	981	813	74	− 72	143	89	94	90	59	21
21	2171	6021	851	24704	33747	443	1269	964	− 83	− 60	166	103	65	109	55	28
22	3046	5830	1201	23697	33774	435	1626	1282	103	− 52	196	130	53	132	53	37
23	3654	6219	1462	22459	33794	423	1703	1698	898	− 113	264	157	78	155	55	45
24	3890	6879	1332	21521	33622	412	990	1315	514	− 54	353	181	90	211	57	47
25	4044	7510	1132	21280	33966	408	545	730	340	− 166	357	152	137	268	62	45
26	3809	8664	1077	21409	34959	407	402	391	237	− 256	342	63	237	302	73	46
27	4259	8950	1158	21573	35940	407	247	259	− 324	− 15	327	7	263	357	75	54
28	4216	10921	932	22267	38336	410	− 273	117	− 1137	− 180	231	27	485	407	103	53
29	6613	10099	1040	22600	40352	412	635	− 457	− 6574	462	146	79	395	713	96	78
30	11339	6722	2182	21403	41646	408	2409	857	373	− 287	174	124	151	1613	57	147
31	12395	9422	2070	20734	44621	395	363	− 1182	539	801	321	55	251	2707	76	188
5-26 (mean)	1447	5795	524	25318	33084	448	648	642	273	− 72	119	74	56	90	55	19

One approach which suggests itself is a comparison between the forecast changes of energy forms, K', $\overline{K}$, P', $\overline{P}$, and the changes in these quantities implied by the finite-difference evaluation of the various energy transformations. Although the continuous equations Eqs. (17)-(19) have the exact energy integrals, Eqs. (39)-(42), the finite-difference equations (see the appendix) do not, and the disagreement between the 'observed' changes in energy and those computed from the energy-transformation functions may then be taken as a partial measure of the importance of truncation error. Such a comparison is also of immediate interest concerning the validity of the energy transformations themselves.

In Table 8 are listed the 24-hr changes in the 'observed' total energy $\Delta E = \Delta(K' + \overline{K} + P' + \overline{P})$, together with the corresponding changes computed from the finite-difference form of the energy budget Eq. (43). Each of the latter values was obtained by adding up the energy transformations concerned at n days and at $n + 1$ days, and then dividing by two to get the 'computed' change in E from n to $n + 1$ days. If we look at the differences, we see that they are rather less than the typical value of $\{\overline{Q} \cdot \overline{P}\}$ (448 units) until about 23-24 days. In the early days, when the disturbance was small and the motion therefore rather linear in character, the agreement is remarkably good. As the disturbance increases in size and K' begins to approach $\overline{K}$ in magnitude, the disagreement increases.

TABLE 8. 24-HR CHANGES IN TOTAL ENERGY OBSERVED (ΔE) AND COMPUTED FROM EQ. (43).

Period (days)	ΔE	E Budget	Difference
0- 1	6	− 10	16
1- 2	261	238	23
2- 3	342	336	6
3- 4	379	372	7
4- 5	388	388	0
5- 6	399	395	4
6- 7	393	392	1
7- 8	383	383	0
8- 9	349	364	− 15
9-10	322	334	− 12
10-11	287	290	− 3
11-12	207	227	− 20
12-13	123	153	− 30
13-14	26	94	− 68
14-15	2	80	− 78
15-16	46	96	− 50
16-17	85	101	− 16
17-18	143	74	69
18-19	187	23	164
19-20	75	− 26	101
20-21	− 57	− 65	8
21-22	27	− 125	152
22-23	20	− 249	269
23-24	− 172	− 429	257
24-25	344	− 570	914
25-26	993	− 635	1628
26-27	981	− 666	1647
27-28	2396	− 786	3182
28-29	2016	− 995	3011
29-30	1294	− 1476	2770
30-31	2975	− 2531	5506

The sign of the disagreement shows a surprisingly slow variation with time, but no explanation for this phenomenon has yet been found. A similar examination of the *individual* energy budgets for K', $\overline{K}$, P' and $\overline{P}$ showed that most of the fictitious energy increase in the last ten days occurred in $\overline{K}$, except in the last three days, where it occurred mainly in K'. After about 25 days, the field of $\overline{u}_1$ contains several places where minimum and maximum values of $\overline{u}_1$ occur at neighbouring grid points (Fig. 13), so that the breakdown of the finite-difference scheme is not surprising.

This breakdown of the computations can presumably be postponed by taking smaller values of Δx and Δy, but this will not eliminate the difficulty completely, and at the same time will require smaller time steps to satisfy the computational stability criterion. Somewhat the same type of disadvantage also appears if higher-order differences are introduced in an attempt to obtain more accurate derivatives. It was thought initially that the introduction of a lateral eddy-viscosity into the equations would eliminate some of the bad effects of truncation errors, by smoothing out the small-scale motions. To some extent this was true, since the computation incorporating A could be carried farther than the check computation with $A = 0$, but evidently a still more fundamental modification of the equations is required.

10. Conclusions

The experiment has succeeded in several aspects; it has predicted the easterly-westerly-easterly distribution of surface zonal wind, the existence of a jet, and the required net poleward transport of energy. Furthermore, the energy-transformation processes which produced these phenomena agree qualitatively with what little is known of the principal energy transformations in the atmosphere. Considering the simplicity of the model, these modest successes are quite gratifying.

There are failures in some of the details; the relative strength of the sub-tropical easterlies compared to those in polar latitudes was not predicted, and the mean latitudinal temperature gradient was too large. Certain features of the disturbance were also not very realistic. However, there is good reason to believe that these failures are merely results of the extreme simplicity of the equations that were used, and will be corrected when more accurate equations are employed.

Certain of the assumptions in this particular numerical experiment can be eliminated in a rather straightforward manner, e.g. the geostrophic assumption and the simplified geometry. However, a further refinement of the model will soon run into the more difficult physical problems of small-scale turbulence and convection, the release of latent heat, and the dependence of radiation on temperature, moisture, and cloud. Progress in the past in developing an adequate theory of the general circulation has had as its main obstacle the difficulty of solving the non-linear hydrodynamical equations. High-speed computing machines have to some extent eliminated this problem, and further progress in understanding the large-scale behaviour of the atmosphere should come to depend more and more on a fuller understanding of the physical processes mentioned above.

Acknowledgments

The research carried out was sponsored by the Office of Naval Research and the Geophysics Research Directorate.

The writer also wishes to acknowledge the invaluable assistance of the staff of the Electronic Computer Project at the Institute for Advanced Study, especially Dr. H. H. Goldstine for his contribution to the solution of some of the numerical problems, and Mr. Glenn Lewis for his help in the design of an efficient code. The experiment is a natural extension of the work by Dr. J. Charney on numerical prediction, and has benefited greatly from his interest and encouragement.

Appendix

1. The numerical forecasting procedure

The forecasting procedure replaces the continuous independent variables by the discrete variables i, j, τ, according to the scheme

$$x = i\,\Delta x \qquad (i = 0, 1, 2, \ldots, I-1)$$

$$y = j\,\Delta y \qquad (j = 0, 1, 2, \ldots, J)$$

$$t = \tau\,\Delta t \qquad (\tau = 0, 1, 2, \ldots.)$$

$i = 0$ corresponds to $x = 0$ and $i = I$ corresponds to $x = L$. $j = 0$ corresponds to $y = -W$, and $j = J$ to $y = +W$.

To describe the numerical process we first define the finite difference operators $\mathcal{L}$ and $\mathcal{J}$ as follows (ϵ is the ratio $\Delta x/\Delta y$) :

$$\Delta x^2\,\nabla^2 S \simeq \mathcal{L}_{ij}\,S = S_{i+1\,j} + S_{i-1\,j} - 2\,S_{ij} + \epsilon^2\,(S_{i\,j+1} + S_{i\,j-1} - 2\,S_{ij})$$

$$4\Delta x\,\Delta y\,\mathcal{J}\left(\frac{R, S}{x, y}\right) \simeq \mathcal{J}_{ij}(R, S) = (R_{i+1\,j} - R_{i-1\,j})\,(S_{i\,j+1} - S_{i\,j-1}) - (R_{i\,j+1} - R_{i\,j-1})\cdot$$
$$\cdot\,(S_{i+1\,j} - S_{i-1\,j}).$$

It is convenient to introduce also the non-dimensional constant

$$\gamma = \lambda^2\,\Delta x^2$$

and to replace the potential vorticities q by

$$\eta_{ij} = q_{ij}\,\Delta x^2.$$

If we then form the finite-difference equivalent of our definition of the x-mean, Eq. (26),

$$\overline{\psi}_{j\tau} = I^{-1} \sum_{i=0}^{I-1} \psi_{ij\,\tau} \qquad . \qquad . \qquad . \qquad . \qquad \text{(A1)}$$

$$\psi'_{ij\tau} = \psi_{ij\tau} - \overline{\psi}_{j\tau}, \qquad . \qquad . \qquad . \qquad . \qquad \text{(A2)}$$

Eqs. (22) and (23) can be written as the following four equations (for convenience we suppress here the τ subscript) :

$$\mathcal{L}_{ij}\,\psi_1' - \gamma\,(\psi_1' - \psi_3')_{ij} - \eta'_{1ij} = 0, \qquad . \qquad . \qquad . \qquad . \qquad \text{(A3)}$$

$$\mathcal{L}_{ij}\,\psi_3' + \gamma\,(\psi_1' - \psi_3')_{ij} - \eta'_{3ij} = 0, \qquad . \qquad . \qquad . \qquad . \qquad \text{(A4)}$$

$$\epsilon^2\,(\overline{\psi}_{1\,j+1} + \overline{\psi}_{1\,j-1} - 2\overline{\psi}_{1j}) - \gamma\,(\overline{\psi}_{1j} - \overline{\psi}_{3j}) - \overline{\eta}_{1j} = 0, \qquad . \qquad \text{(A5)}$$

$$\epsilon^2\,(\overline{\psi}_{3\,j+1} + \overline{\psi}_{3\,j-1} - 2\overline{\psi}_{3j}) + \gamma\,(\overline{\psi}_{1j} - \overline{\psi}_{3j}) - \overline{\eta}_{3j} = 0. \qquad . \qquad \text{(A6)}$$

Given η_1' and η_3', Eqs. (A3) and (A4) determine ψ_1' and ψ_3' in the interior ($0 \leqslant i \leqslant (I-1)$, $1 \leqslant j \leqslant (J-1)$) if we use the boundary conditions

$$\psi'(i, j) = 0 \qquad \text{at} \qquad j = 0 \qquad \text{and} \qquad J, \qquad . \qquad . \qquad . \qquad \text{(A7)}$$

$$\psi'(0, j) = \psi'(I, j), \qquad \psi'(-1, j) = \psi'(I-1, j). \qquad . \qquad . \qquad \text{(A8)}$$

These are equivalent to Eq. (28) and the cyclic boundary condition. The two equations, (A3) and (A4), are then easily solved for ψ' by relaxation techniques (Charney and Phillips 1953).

The solution of the *ordinary* difference equations (A5) and (A6) for $\overline{\psi}_j$, when $\overline{\eta}_j$ is known, uses the boundary conditions

$$\left.\begin{aligned}\overline{\psi}(j=J) &= \overline{\psi}(j=J-1),\\ \overline{\psi}(j=0) &= \overline{\psi}(j=1),\end{aligned}\right\} \quad . \quad . \quad . \quad \text{(A9)}$$

together with one extra condition; for example,

$$\overline{\psi}_3(j=0) = 0. \quad . \quad . \quad . \quad . \quad . \quad \text{(A10)}$$

Solution of Eqs. (A5) and (A6) by conventional relaxation methods is not very satisfactory; their one-dimensional character and the boundary conditions (A9) do not make for very rapid convergence of the iterative process. Furthermore, a rather accurate solution is required, if the computation of $\overline{\omega}_{2j}$ from Eq. (A18) is to be at all accurate. They can be solved ' exactly ' by using a finite-difference analogue of a Green's function, but this involves either (a) a tabulation of a rather large number of Green's function values (of the order of $\frac{1}{2}J^2$), or, (b) the computation of the Green's function as needed from products of the form a^j and a^{-j}, whose scaling becomes awkward. Dr. H. Goldstine of the Institute for Advanced Study suggested a method to the writer which was free from these objections, and which proved to be extremely satisfactory with respect to accuracy, speed of computation, and size of the code needed. The method is applicable to a somewhat wider class of ordinary difference equations, and will be described by Goldstine and von Neumann at a later time.

The usual technique employed in numerical forecasting in forming a finite difference equivalent of (24)-(25) is to evaluate the right side of those equations at time τ and express the left side as a centred difference $(q_{ij\,\tau+1} - q_{ij\,\tau-1})/2\Delta t$ (after a single uncentred step at the very beginning). However, it can be shown that in our case this procedure is not stable because of the frictional terms involving A and k; if they are evaluated at τ, they give rise to both exponentially amplified and damped solutions, whereas only the damped solution is real. This difficulty can be overcome either by evaluating the frictional terms (explicitly and uncentred) at $\tau - 1$, or (implicitly and centred) as an average at $\tau - 1$ and $\tau + 1$. The latter method is slightly more accurate and formed the basis of the scheme employed in the calculations.

The actual finite-difference forms used for Eqs. (24) and (25) were the following:

$$\left.\begin{aligned}\left[-\alpha\mathcal{L}+1\right]\eta_{1ij\,\tau+1} = x_{1ij} = \eta_{1ij\,\tau-1} &+ c\mathcal{J}_{ij}(bj+\eta_1,\psi_1)_\tau +\\ &+ \alpha\mathcal{L}\eta_{1ij\,\tau-1} + h(2j-J)/J,\end{aligned}\right\} \quad . \quad \text{(A11)}$$

$$\left.\begin{aligned}\left[-\alpha\mathcal{L}+1+\frac{3k\Delta t}{2}\right]\eta_{3ij\,\tau+1} = x_{3ij} = \eta_{3ij\,\tau-1} &+ c\mathcal{J}_{ij}(bj+\eta_3,\psi_3)_\tau +\\ &+ \alpha\mathcal{L}\eta_{3ij\,\tau-1} - h(2j-J)/J +\\ &+ k\Delta t\left[\tfrac{3}{2}\eta_{3\,\tau-1} - \eta_{1\tau} - 4\gamma(\psi_1-\psi_3)_\tau\right]_{ij},\end{aligned}\right\} \quad . \quad \text{(A12)}$$

where $\alpha = A\,\Delta t/(\Delta x)^2, \quad b = \beta\,\Delta x^2\,\Delta y, \quad c = \Delta t/2\,\Delta x\,\Delta y,$

and $h = 4RH\,\gamma\,\Delta t/f_0\,c_p.$

The lateral diffusion terms $A\,\nabla^2\eta$ were thus evaluated completely implicitly while the surface friction term $-k\zeta_4$ was evaluated partly implicitly and partly explicitly.

The computation stability criterion, which sets an upper limit to the allowable time step Δt, in the absence of the frictional terms can be written

$$c\,(|\psi_{i+1\,j} - \psi_{i-1\,j}| + |\psi_{i\,j+1} - \psi_{i\,j-1}|) < 1. \quad . \quad . \quad \text{A13)}$$

The frictional term makes this restriction more severe, but for the small values of A and k we are using (for $\Delta t = 1$ hr and $\Delta x = 375$ km, $\alpha = 0{\cdot}00256$ and $k\Delta t = 0{\cdot}0144$) this is only a small effect, and the computations remain stable if we replace 1 in (A13) by, say, 0·95. The code was then designed to apply the test (A13) at every point, and to stop if the criterion was exceeded. (This is easily done during the computation of χ in Eqs. (A11) and (A12).) The largest value of the left side of (A13) that had been reached so far in the computation was also periodically printed out every 24 hr, making it possible to shorten the time step before (A13) was violated.

The solution of the implicit Eqs. (A11) and (A12) for $\eta_{ij\,\tau+1}$ proceeds in two steps: first, the straightforward computation of χ_{ij}, and second, the inversion of the two equations (s taking on the values 1 and 3)

$$\left[\alpha\mathcal{L}_{ij} - \mu_s\right] \eta_{sij\,\tau+1} = -\chi_{sij} \quad . \quad . \quad . \quad \text{(A14)}$$

for $\eta_{sij\,\tau+1}$, where $\mu_s = 1$ for $s = 1$ and $\mu_s = 1 + \frac{3}{2}k\Delta t$ for $s = 3$. This last process was in turn divided up into two steps,

$$\left[\alpha\mathcal{L}_{ij} - \mu_s\right] \eta'_{sij\,\tau+1} = -\chi'_{sij}, \quad . \quad . \quad . \quad \text{(A15)}$$

$$\alpha\epsilon^2\,(\bar{\eta}_{j+1} + \bar{\eta}_{j-1} - 2\bar{\eta}_j)_{s\,\tau+1} - \mu_s\,\bar{\eta}_{sj\,\tau+1} = -\bar{\chi}_{sj}, \quad . \quad . \quad \text{(A16)}$$

by again introducing the finite-difference means analogous to Eqs. (A1) and (A2). Eq. (A15) was solved by relaxation with $\eta' = 0$ at $j = 0$ and $j = J$ and the cyclic boundary condition

$$\eta'\,(i = 0) = \eta'\,(i = I).$$

Eq. (A16) was solved 'exactly,' by the same technique as was used for Eqs. (A5) and (A6), with the boundary conditions,

$$\left.\begin{aligned} &\bar{\eta}\,(j = 0) = \bar{\eta}\,(j = 1), \\ &\bar{\eta}\,(j = J) = \bar{\eta}\,(j = J - 1). \end{aligned}\right\} \quad . \quad . \quad . \quad \text{(A17)}$$

Finally $\eta_{ij\,\tau+1}$ was obtained by adding η' and $\bar{\eta}$.

The general computational scheme, then, proceeded very much as described by Charney and Phillips (1953), the 'history' of the motion being carried by the η's, with the ψ's being determined from (A3)-(A6) at each time step after the η's had been extrapolated forward in time by (A11)-(A12). The only variation from conventional schemes was the partially implicit character of Eqs. (A11) and (A12), necessitating an additional inversion of an elliptic partial difference equation.

The extrapolated Liebman process (Charney and Phillips 1953) was used in the relaxation solution of Eqs. (A3), (A4) and (A15). The initial guess, $<\psi'_{ij\,\tau+1}>$, for $\psi'_{ij\,\tau+1}$ in Eqs. (A3) and (A4) was obtained by the formula

$$<\psi'_{ij\,\tau+1}> = 2\,\psi'_{ij\tau} - \psi'_{ij\,\tau-1}.$$

In order to do this, it was necessary to store the otherwise unused values of $\psi'_{\tau-1}$, but the resulting increase in the speed of the computation through the decrease in the required number of iterations in the Liebman process made this very worth while. The relaxation

process for ψ' was carried out until the quantity $|\psi'_{\nu+1} - \psi'_{\nu}|_{1ij} + |\psi'_{\nu+1} - \psi'_{\nu}|_{3ij}$ was everywhere less than $\frac{3}{8} \times 10^5$ m^2 sec^{-1}, about $\frac{3}{8}$ m in units of isobaric height (the subscript ν indicates successive iterative guesses). This took between 3 and 6 iterations, depending on the size of the time step.

The solution of Eq. (A15) by relaxation was very rapid because of the small value of the ratio α/μ. (The optimum over-relaxation process has an eigenvalue of about 10^{-3}.) Here the first guess was $<\eta'> = \mu^{-1} x'$, and very few iterations (< 5) were necessary to reduce the error in η' to less than 600 m^2 sec^{-1} (corresponding to an error in $q = \Delta x^{-2} \eta$ of less than 4×10^{-9} sec^{-1}).

The complete set of computations for one time step took about 50 sec. About 18 sec were spent in the computation of $x_{\tau+1}$, 2 sec in the solution of (A16), 8 sec in (A15), 2 sec in the solution of (A5) and (A6), and 20 sec in the solution of (A3) and (A4).

The η's and the ψ's were both stored as 20 binary-digit numbers; the scaling being such that the round-off error in storing η corresponded to an error of about $\pm 2 \times 10^{-9}$ sec^{-1} in q, and that incurred in storing ψ corresponding to an error in isobaric height of about $\pm 0{\cdot}006$ m. As far as is known, round-off errors of this type did not influence the computations to any significant degree.

A time step of 2 hr was used until $t = 8$ days, one of $1\frac{1}{2}$ hr until $t = 12$ days, one of 1 hr until $t = 23$ days, and the forecast was finished using a time step of $\frac{1}{2}$ hr. The 31-day forecast thus required a total of 812 time steps. Whenever the time step was shortened at time t from Δt to $\Delta t'$, values of $\eta_{\tau-1} = \eta(t - \Delta t')$ for the first computation of Eqs. (A11) and (A12) with the new time step were obtained by interpolation from the values of $\eta(t)$ and $\eta(t - \Delta t)$.

The forecasting code proper, which solved (A3)-(A6) and (A11)-(A12) required almost 2,000 separate instructions and constants. The computation of the energy terms, meridional circulation, $\bar{u}$, $\overline{T}_2$, etc., required about 1,700 separate instructions, almost as much as the forecast code itself. An additional 3,000 instructions were used to perform miscellaneous tasks, e.g., the formation of the initial ψ and η fields at $t = 0$, the interpolation necessary when the time step was changed, and the computation of the preliminary forecast without eddies.

2. Numerical evaluation of the energy parameters and the meridional circulation

In general, the finite-difference evaluation of the energy functions is somewhat arbitrary, since the finite-difference forecast equations (A3)-(A6) and (A11)-(A12) do not possess exact energy integrals, and therefore do not lead automatically to a specification of the proper way to evaluate the functions using ψ values at only two time steps. (This is true even of the simplest barotropic vorticity equation $\nabla^2 \partial\psi/\partial t = -\mathbf{V} \cdot \nabla\nabla^2 \psi$ in the finite-difference form by which it has hitherto been solved, (e.g., Charney, Fjørtoft, and von Neumann 1950).) Therefore, the following formulae will be for the most part simply listed, with little or no justification being given for the particular form employed.

For simplicity we introduce the abbreviated notation for the sums

$$\mathrm{X}\, S_{ij} = I^{-1} \sum_{i=0}^{I-1} S_{ij},$$

$$\mathrm{Y}\, S_{ij} = J^{-1} \sum_{j=1}^{J-1} S_{ij}.$$

At 24-hourly intervals, a record was made of the two latest ψ-fields, $\psi_{ij\tau}$ and $\psi_{ij\,\tau-1}$, at

levels 1 and 3. These were then averaged and differenced to form

$$\delta\psi_{ij} = \psi_{ij\tau} - \psi_{ij\,\tau-1},$$
$$\psi_{ij}^{*} = \tfrac{1}{2}(\psi_{ij\tau} + \psi_{ij\,\tau-1}),$$

and these new quantities were used throughout in the computation of the energy parameters and the meridional circulation. For convenience, the asterisk will be dropped from now on, ψ_{ij} always implying ψ_{ij}^{*}.

ω_2 was determined from the finite-difference form of Eq. (19):

$$\omega_{2ij} = \frac{\lambda^2 p_2}{f_0}\left[\frac{(\delta\psi_1 - \delta\psi_3)_{ij}}{\Delta t} - \frac{\mathcal{J}_{ij}(\psi_1, \psi_3)}{4\,\Delta x\,\Delta y} + \frac{2RH(2j-J)}{f_0 c_p J} - \frac{A}{\Delta x^2}\mathcal{L}(\psi_1 - \psi_3)\right] \quad . \quad \text{(A18)}$$

The meridional circulation was determined by the equation

$$\overline{V}_{1\,j+\frac{1}{2}} = \overline{V}_{1\,j-\frac{1}{2}} - \frac{\Delta y}{p_2}\,\overline{\omega}_{2j}, \qquad j = 1, 2, \ldots, J-1, \quad . \quad . \quad \text{(A19)}$$

with $\overline{V}_1 = 0$ at $j = \frac{1}{2}$, and $\overline{\omega}_{2j}$ being given by $\mathrm{X}\,\omega_{2ij}$. The smallness of $\overline{V}_1$ at $j = J - \frac{1}{2}$ is a fairly severe test of the effect of round-off error in the computations, the exact *finite-difference* solution leading to a zero value for $\overline{V}_1$ and $\overline{V}_3$ at $j = J - \frac{1}{2}$. The average value of $|\overline{V}_{1\,J-\frac{1}{2}}|$ was about 5 mm sec^{-1} during the 31-day forecast, i.e., about 1 per cent of the maximum values of $\overline{V}_1$ away from the walls.

The kinetic energies were computed from the formulae

$$K' = \frac{10}{2J\,\Delta x^2}\sum_{j=0}^{J-1}\mathrm{X}\{[(\psi'_{i+1} - \psi'_i)^2{}_{1j} + (\psi'_{i+1} - \psi'_i)^2{}_{3j}] + \epsilon^2[(\psi'_{j+1} - \psi'_j)^2{}_{1i} + (\psi'_{j+1} - \psi'_j)^2{}_{3i}]\},$$

$$\overline{K} = \frac{10}{2\,\Delta y^2}\,\mathrm{Y}\,[(\overline{\psi}_{j+1} - \overline{\psi}_j)_1{}^2 + (\overline{\psi}_{j+1} - \overline{\psi}_j)_3{}^2], \quad . \quad . \quad . \quad . \quad . \quad \text{(A20)}$$

and the potential energies from

$$\left.\begin{aligned} P' &= \frac{10\,\lambda^2}{2}\,\mathrm{Y}\,\mathrm{X}\,(\psi_1' - \psi_3')^2{}_{ij}, \\ \overline{P} &= \frac{10\,\lambda^2}{2}\,\mathrm{Y}\,(\overline{\psi}_1 - \overline{\psi}_3)^2{}_j. \end{aligned}\right\} \quad . \quad . \quad . \quad \text{(A21)}$$

The eleven energy transformations had the formulae :

$$\{\overline{Q}\cdot\overline{P}\} = -\frac{2RH\lambda^2 l}{f_0 c_p}\,\mathrm{Y}\,\frac{2j-J}{J}\,(\overline{\psi}_1 - \overline{\psi}_3)_j$$

$$\{\overline{P}\cdot P'\} = -\frac{\lambda^2 l}{4\,\Delta x\,\Delta y}\,\mathrm{Y}\,[(\overline{\psi}_1 - \overline{\psi}_3)_j\,\mathrm{X}\,\mathcal{J}(\psi_1', \psi_3')_{ij}]$$

$$\{P'\cdot K'\} = -\frac{f_0 l}{p_2}\,\mathrm{Y}\,\mathrm{X}\,\omega'_{2ij}\,(\psi_1' - \psi_3')_{ij}$$

$$\{K'\cdot\overline{K}\} = \frac{l}{4\,\Delta x^3\,\Delta y}\,\mathrm{Y}\,\{[(\overline{\psi}_{j-1} - \overline{\psi}_{j+1})\,\mathrm{X}\,(\psi'_{i+1} - \psi'_{i-1})_j\,\mathcal{L}\,\psi'_{ij}]_1 + [(\overline{\psi}_{j-1} - \overline{\psi}_{j+1})\,\mathrm{X}\,(\psi'_{i+1} - \psi'_{i-1})_j\,\mathcal{L}\,\psi'_{ij}]_3\}$$

$$\{\overline{P}\cdot\overline{K}\} = -\frac{f_0 l}{p_2}\,\mathrm{Y}\,\overline{\omega}_{2j}\,(\overline{\psi}_1 - \overline{\psi}_3)_j$$

$$\{\overline{K}\cdot A\} = Al\,\mathrm{Y}\,(\overline{\zeta}_1{}^2 + \overline{\zeta}_3{}^2)_j$$

$$\{K'\cdot A\} = Al\,\mathrm{Y}\,\mathrm{X}\,[(\zeta'_{1ij})^2 + (\zeta'_{3ij})^2]$$

$$\{\overline{P}\cdot A\} = \frac{\lambda^2 Al}{\Delta y^2}\,\mathrm{Y}\,[(\overline{\psi}_1-\overline{\psi}_3)_{j+1}-(\overline{\psi}_1-\overline{\psi}_3)_j]^2$$

$$\{P'\cdot A\} = \frac{\lambda^2 Al}{J\,\Delta x^2}\sum_{j=0}^{J-1}\mathrm{X}\{[(\psi_1'-\psi_3')_{i+1}-(\psi'_1-\psi_3')_i]_j^2+\epsilon^2[(\psi_1'-\psi_3')_{j+1}-(\psi_1'-\psi_3')_j]_i^2\}$$

$$\{\overline{K}\cdot k\} = -\,kl\,\mathrm{Y}\,\overline{\zeta}_{4j}\,\overline{\psi}_{3j}$$

$$\{K'\cdot k\} = -\,kl\,\mathrm{Y}\,\mathrm{X}\,\zeta'_{4ij}\,\psi'_{3ij}$$

Here $l = 10$ days $= 8{\cdot}64 \times 10^5$ sec and $\zeta_{ij} = \Delta x^{-2}\,\mathcal{L}_{ij}\,\psi$. The units for the four energies and the eleven energy transformations will then be the same as those in the tables in the text if the dimensional quantities in the above formulae are measured in the metre-ton-second system. (The formula for $\{K'\cdot\overline{K}\}$ uses the relationship $\overline{v\zeta} = -\,\partial\,(\overline{uv})/\partial y$ which is valid when u and v are given by a stream function.)

3. Numerical values of the physical constants

The constants appearing in the equations had the following values :

$$H = 2 \times 10^{-3}\ \mathrm{kj\ ton^{-1}\ sec^{-1}}\ (2 \times 10^{-6}\ \mathrm{j\ g^{-1}\ sec^{-1}})$$

$$\lambda^2 = f_0^2\,\theta_2\,[(\theta_1-\theta_3)\,(\phi_1-\phi_3)]^{-1} = 1{\cdot}5 \times 10^{-12}\ \mathrm{m^{-2}}$$

$$\Delta x = 375\ \mathrm{km}$$

$$\Delta y = 625\ \mathrm{km}$$

$$R = 287\ \mathrm{kj\ ton^{-1}\ deg^{-1}}$$

$$c_p = 1004\ \mathrm{kj\ ton^{-1}\ deg^{-1}}$$

$$A = 10^5\ \mathrm{m^2\ sec^{-1}}\ \text{(zero in check computation)}$$

$$k = 4 \times 10^{-6}\ \mathrm{sec^{-1}}$$

$$\beta = 1{\cdot}6 \times 10^{-11}\ \mathrm{sec^{-1}\ m^{-1}}$$

$$p_2 = \tfrac{1}{2}\,p_4 = 500\ \mathrm{mb}$$

$$I = J = 16$$

The value for λ^2 comes from values of

$$f_0 = 10^{-4}\ \mathrm{sec^{-1}}$$

$$\phi_1-\phi_3 = 77{,}499\ \mathrm{m^2\ sec^{-2}}$$

$$\theta_2/(\theta_1-\theta_3) = 11{\cdot}625$$

(The last value is slightly larger than that occurring in the standard atmosphere, to allow qualitatively for the destabilizing effect of the release of latent heat.)

References

Albrecht, F.	1931	*Met. Z.*, **48**, p. 57.
Arakawa, H.	1953	*J. Met.*, **10**, p. 392.
Batchelor, G. K.	1950	*Quart. J. R. Met. Soc.*, **76**, p. 133.
Baur, F. and Philipps, H.	1935	*Beitr. Geophys.*, **45**, p. 82.

Benson, G. S. and Estoque, M. A.	1954	*J. Met.*, **11**, p. 462.
Bjerknes, V., Bjerknes, J., Solberg, H. and Bergeron, T.	1933	*Physikalische Hydrodynamik*, Berlin (J. Springer).
Blackadar, A. K.	1955	*J. Met.*, **12**, p. 165.
Brunt, D.	1944	*Physical and dynamical meteorology*, Cambridge University Press.
Charney, J.	1947	*J. Met.*, **4**, p. 135.
	1951	*U.G.G.I. Ass. Met. Compte Rendu*, Brussels, p. 47.
	1954	*Proc. Nat. Acad. Sci.*, **40**, p. 99.
	1955	Unpublished.
Charney, J. and Eliassen, A.	1949	*Tellus*, **1**, No. 2, p. 38.
Charney, J., Fjørtoft, R. and von Neumann, J.	1950	*Ibid.*, **2**, p. 237.
Charney, J. and Phillips, N.	1953	*J. Met.*, **10**, p. 71.
Defant, A.	1921	*Geog. Ann.*, Stockholm, **3**, p. 209.
Eady, E. T.	1949	*Tellus*, **1**, No. 3, p. 33.
	1950	*Cent. Proc. R. Met. Soc.*, p. 156.
Eliassen, A.	1949	*Geofys. Publ.*, Oslo, **17**, No. 3.
	1952	*Astrophys. Norveg.*, Oslo, **5**, No. 2.
Exner, F.	1925	*Dynamische meteorologie*, Vienna (J. Springer).
Fjørtoft, R.	1950	*Geofys. Publ.*, Oslo, **17**, No. 6.
	1951	*Compendium Met., Amer. Met. Soc.*, p. 454.
Fultz, D.	1951	*Ibid.*, p. 1235.
Gabites, J. F.	1950	Doctoral thesis, M.I.T.
Grimminger, G.	1938	*Trans. Amer. Geophys. Un.*, **19**, p. 163.
Hadley, G.	1735	*Phil. Trans. Roy. Soc.*
Hess, S.	1948	*J. Met.*, **5**, p. 293.
Hide, R.	1953	*Quart. J. R. Met. Soc.*, **79**, p. 161.
Houghton, H.	1954	*J. Met.*, **11**, p. 1.
Høiland, E.	1939	*Arch. Math. Naturv.*, **42**, No. 5.
Jeffreys, H.	1926	*Quart. J. R. Met. Soc.*, **52**, p. 85.
Kuo, H. L.	1952	*J. Met.*, **9**, p. 260.
	1953	*Ibid.*, **10**, p. 235.
	1954	*Ibid.*, **11**, p. 399.
Lamb, H.	1932	*Hydrodynamics*, 6th Ed., Cambridge University Press.
London, J.	1951	*Progr. Rep. Dept. Met., New York Univ.*, No. 131.07.
Lorentz, E. N.	1955	*Tellus*, **7**, p. 157.
Machta, L.	1955	Paper presented at 135th national meeting Amer. Met. Soc., New York (Abstract in *Bull. Amer. Met. Soc.*, **35**, p. 493).
Mintz, Y.	1954	*Bull. Amer. Met. Soc.*, **35**, p. 208.
	1955	'Investigations of the general circulation of the atmosphere,' final report, Dept. Met., Calif. Univ., Los Angeles.
Möller, F.	1950	*Experientia*, **6**, p. 361.
Palmén, E.	1951	*Compendium Met., Amer. Met. Soc.*, p. 599.
	1955	'Investigations of the general circulation of the atmosphere,' final report, Dept. Met., Calif. Univ., Los Angeles.
Palmén, E. and Alaka, M. A.	1952	*Tellus*, **4**, p. 324.
Palmén, E. and Newton, C.	1951	*J. Met.*, **8**, p. 25.
Phillips, N.	1949	*Ibid.*, **6**, p. 193.
	1954	*Tellus*, **6**, p. 273.
Richardson, L. F.	1926	*Proc. Roy. Soc.*, A, **110**, p. 709.
Riehl, H. and Yeh, T. C.	1950	*Quart. J. R. Met. Soc.*, **76**, p. 182.
Rossby, C.-G. and collaborators	1939	*J. Mar. Res.*, New Haven, **2**, p. 38.
Sheppard, P. A.	1953	*Proc. Toronto Met. Conf., R. Met. Soc.*, p. 103.
Sheppard, P. A., Charnock, H. and Francis, J. R. D.	1952	*Quart. J. R. Met. Soc.*, **78**, p. 563.
Simpson, G. C.	1929	*Mem. R. Met. Soc.*, **3**, No. 23, p. 53.
Spar, J.	1950	*J. Met.*, **7**, p. 48.
Staff members, Dept. Met., Chicago Univ.	1947	*Bull. Amer. Met. Soc.*, **28**, p. 255.
Starr, V. P.	1951	*Compendium Met., Amer. Met. Soc.*, p. 568.
	1953	*Tellus*, **5**, p. 494.
	1954	*Ibid.*, **6**, p. 268.
Starr, V. P. and White, R.	1955	'Studies of the atmospheric general circulation,' final report, Dept. Met., M.I.T., p. 186.
van Mieghem, J.	1952	*Tellus*, **4**, p. 334.
Widger, W.	1949	*J. Met.*, **6**, p. 291.